CHALMERS
UNIVERSITY OF TECHNOLOGY

Development of a Predictive Maintenance Algorithm for Detection of Faulty Drive Belts

Master's thesis in Systems, Control and Mechatronics

VIKTOR EKLIND and JONATHAN KARLSSON

Department of Electrical Engineering
CHALMERS UNIVERSITY OF TECHNOLOGY
Gothenburg, Sweden 2018

Master's thesis EX83/2018

Development of a Predictive Maintenance Algorithm for Detection of Faulty Drive Belts

In cooperation with Mobile Climate Control

Viktor Eklind

Jonathan Karlsson

CHALMERS
UNIVERSITY OF TECHNOLOGY

Department of Electrical Engineering
Chalmers University of Technology
Gothenburg, Sweden 2018

Development of a Predictive Maintenance Algorithm for Detection of Faulty Drive Belts

Supervisor: Tina Mirfakhraie, Mobile Climate Control
Examiner: Tomas Mckelvy

Master's Thesis EX83/2018
Department of Electrical Engineering
Signal Processing
Chalmers University of Technology
SE-412 96 Gothenburg
Telephone +46 31 772 1000

Typeset in LaTeX
Gothenburg, Sweden 2018

Development of a Predictive Maintenance Algorithm for Detection of Faulty Drive Belts

VIKTOR EKLIND, JONATHAN KARLSSON
Department of Electrical Engineering
Chalmers University of Technology

Abstract

This thesis covers the development of a service dedicated to predictive maintenance of a power transmission belt. In particular, the belt's tension is assumed to be the most important attribute when it comes to its need for maintenance and will therefore be the main focus. Predictive maintenance is desirable since it allows the owner of equipment to maximize its value generating time. Characteristics that are related to belt tension includes; heat development caused by increased friction, slippage due to loss of traction and vibrations of the belt related to its tension. These three attributes are utilized when developing 4 different methods in order to make conclusions about the belt's tension. First it is investigated how slip can be detected and related by looking at speed ratios of a motor and a compressor followed by a temperatures model that is derived using available measurements and by estimating system parameters from collected data. Some effort is put into analyzing the vibrations in the system using a vibration model to detect frequencies that are related to the belt's tension. The statistical moment kurtosis is finally used for time domain analysis of the vibration data to detect anomalies in the system. The methods are developed and tested with experiments on a test rig that was designed and built for this work. In the end the methods are compared to each other on data that attempts to mimic realistic conditions. It turns out that slip is the simplest and also the best method of the ones included. The other methods perform worse and the attempt to find the belt's tension related to vibrations completely shows lack of results. Future attempts to advance in this field should focus on a deeper understanding of one single method and use data from a complete belt life cycle.

Keywords: predictive maintenance, belt drive, test rig, test design, sensors, accelerometer.

Acknowledgements

Firstly we would like to thank Tomas McKelvey for taking on the role as the examiner of the project. We would like to thank Tina Mirfakhraie for the supervisory role at Mobile Climate Control, giving feedback on ideas and proposing solutions. We would also like to thank Chadwick Cuirrier for the help with the construction of the test rig and Brent Griffith for helping with the setup of the data acquisition system.

Viktor Eklind and Jonathan Karlsson, Gothenburg, November 2018

Contents

List of Figures

List of Tables

1

Introduction

1.1 Background

Mobile Climate Control (MCC) is a provider of climate systems for commercial vehicles, with the biggest group of end-users in the public transit industry, i.e buses in city traffic. A common source of failure of these type of systems is the power transmission belt connecting the compressor to the motor, this results in an immediate compressor stop, which is the single most vital component of the climate system. There are currently two ways to deal with these types of failures, one can schedule the vehicle for periodic maintenance, which is costly and causes unnecessary down-time in the value generating process. The other way is to simply wait for the breakdown and repair only when necessary, which results in unsatisfied customers (for example commuters on a hot bus) and the risk of damaging other components and extra cost of unscheduled repair. MCC currently operates a cloud based surveillance system called *FleetTracker* that monitors many of the parameters important for the air conditioning system. The company's long term goal is to implement a service that can give their customers maintenance recommendations regarding the compressor for example.

Experience from MCC tells that the breakdowns occurs mostly because the drive belt has been run with either too high or too low tension. Any of these two situations may increase the rate of degradation of the belt and shorten its lifetime. Failures can also happen due to other mechanical defects, for instance the pulleys on which the belt runs, can be misaligned, causing increased stress on the components in the system, or worn out bearings may cause excessive heat or vibrations leading to structural fatigue in the long run.

The aim is to detect when a drive belt is operating with a tension that might lead to a belt failure or even damage of other components. In other words, one would like to tell if the belt is too tight or too loose while the system is running, preferably without having to take into account any (or a small amount) of application specific parameters to allow for easy and somewhat universal implementations. The purpose is to be able to schedule maintenance before an actual breakdown occur in order to reduce overall costs and improve customer satisfaction. A concrete goal is to design an algorithm that in run-time can determine if the belt's tension is within its specification just as good as a technician would do in a workshop. The approach taken here is signal based and by comparing signals generated from various running conditions the goal is to find characteristics that can be used to discriminate between a belt with correct and incorrect tension.

The project will focus on problems related to the belt drive connecting an electrical motor with one type of the compressors in MCC's systems. Other faults in the system will not be considered. Furthermore, the project is constrained by a budget that will limit the freedom to choose equipment such as high quality sensors. Some parts of the system which is to be analyzed is not going to be modelled due to the complexity required to capture the dynamics of interest (e.g belt slip and vibrations) and the need to determine many material parameters, decreasing the re-usability of the results. Instead real experiments will be conducted on a full scale system and the following analysis will be of a signal based approach, however some simple and general models are utilized. Where the drive belt in a real system slowly degrades over years, the experiment procedure will involve retensioning of the belts to simulate older and worn belts.

1.2 Previous work

A significant amount of research has been done about preventive and predictive maintenance during the last 100 years. The first works were focusing more on how to prevent failures by ensuring that the correct materials etc were used and the later works are more focusing on how to predict failures. Some simple examples are how the car is warning about low oil levels or that some other functionality is not working properly. These types of warnings are usually triggered by a sensor, detecting abnormal behavior in a system. Many recent works have also examined the possibility to measure the conditions and predicting failures in belt drives which will be similar to this project. The recent release of Mathworks' MATLAB 2018a contains a new "Predictive Maintenance Toolbox", although it is mainly intended to be used as a tool with big data analysis and machine learning, it still shows the relevance for this type of research in modern industry.
In [2] the possibility to do online monitoring of the speed and vibrations in a belt drive was examined. The project included an electrostatic sensor to measure the electrical field induced by a belt, from which a frequency analysis was made to extract valuable information. The setup only included a DC-motor which was driving a pulley. Thus, it was not possible to vary load or tension of the belt. The outcome of the project was that it is possible to estimate speed and vibrations of a belt using an electrostatic sensor.
In [3] the results of vibration measurements done by a microphone array was compared and matched with a laser vibrometer. The laser tool gives accurate data but is expensive, motivating why it would be of interest to compare it against less expensive sensors. The comparison was done on a simple V-belt system and the results show that it is possible to find the belt's frequency content and how the natural frequencies changes with the change of belt tension. The research group also found that there are a big difference between a loose and tight belt in the kurtosis value at every octave of the measured sounds from the belt. Contact with the authors reveals that the matter has not been further investigated but the recommendation is to look at the kurtosis in each octave to determine belt tension.
Several studies covers the possibilities to analyze the current in an electrical motor to make conclusions about the health of the system. In [4], the current in an

electrical motor was analyzed to find anomalies in a pulley of a belt driven system. Fault injection was used to also simulate cracks and wears in belts. The results were positive and showed that it is indeed possible to make predictions by only observing current. Although the experiments in the current work indeed will involve an electrical motor, the future implementation would be exclusively together with combustion engines, hence such analysis are of no particular interest here but are still an interesting branch in this research domain.
In [5] they try to detect a loose belt by analyzing motor vibrations, motor current and belt slip. Most attention is given to the analysis of motor current but in the analysis of belt slip it seems to be easier to spot signs of a loose belt.
To the knowledge of the authors of this current work, there exists no (published) work showing a successful implementation of a system that is being able to on its own make the conclusion whether a drive belt is well tensioned or not. Previous work shows, such as in [3], that it is possible to spot differences between the two cases when compared side-by-side, hence lacking the generality sought here. The most promising method seems to be looking for belt slip, a phenomenon that (if observed) gives an absolute sign of belt tension.

1.3 Outline

In this work the authors will work towards an implementation that is being able to determine belt tension of a power transmission belt in run-time. The main idea is to utilize three main characteristics connected with an ill-tensioned belt, namely belt slip, heat development and belt vibrations. In each of these three domains, at least one method will be developed with the final goal of being able to determine belt tension. The methods are developed and tested on collected data from a set of experiments , covering a wide range of possible operations. In the end the different methods will be compared based on their ability to correctly classify the belt tension based on data from more realistic (less ideal) experiments.
The Theory chapter of this report gives some deeper knowledge about compressor systems and belt drives useful for readers not familiar with the concepts. It also gives some theoretical background about the methods used to analyze the system.
In Methods, the test rig design and the experimental procedure is thoroughly explained together with some specifications of the used hardware and signal filtering techniques.
In Results, the different techniques are tested on collected data and the results of them are presented. The developed methods are verified and evaluated for different operation points followed by a discussion of the results.
In Conclusion, the results are reviewed and the best solutions are highlighted followed by an evaluation of the design steps taken in the project. Furthermore, some suggestions of future research are provided.

2
Theory

This chapter provides background theory of compressor systems and predictive maintenance as well as theory about the different symptoms that will will be under investigation.

2.1 Belt drives

Belt drives have for a long time been a common way to transfer power between a source and a load, relying on the friction between the belt and the surfaces on both sides of the transmission. Applications can be found in all type of industries and ranges from large stationary power transmissions to miniature positioning systems. One everyday example of an application known to most people is the belt drive found in many vehicles powered by an internal combustion engine. Here the belt allows for the transfer of power from the engine to other peripheral systems of the vehicle, such as the air conditioning. A common substitute for the conventional belt, which is usually made out of rubber and reinforced by different polymers or metal cords, is a metal chain connecting power source and load. A mechanical advantage of using belt drive instead of a chain is its elastic properties, this allows for a certain flexibility during torque changes which can spare mechanical parts such as bearings and shafts from unnecessary stress. This advantage also comes with a price, a belt that operates with a non-ideal friction between belt and pulley surface will in best case suffer from occasional slip during load changes and in worse case be subject to substantial constant slipping, decreasing the transmission efficiency and causing the belt to wear out prematurely. The belt and other components in the drive system are designed to tolerate a specific temperature limit, where they might age faster or overheat if the temperatures are exceeded. A general suggestion from belt manufacturers [6] is that belts should operate under $60°C$ to avoid faster degradation where every $10°C$ over $60°C$ increases the effect of aging with 50%.

2.2 Compressor systems

It is common to use a compressor in air conditioning systems when colder air needs to be added to an environment. In Figure 2.1, a cooling system is illustrated. The compressor that is driven by a motor via a belt (5), compresses the refrigerant gas from (4) forcing it into the condenser (1) and turns the refrigerant into a liquid

state, thus releasing energy as heat. A fan then removes heat from the refrigerant in the condenser. The expansion valve regulates the amount of fluid that enters the evaporator from (2). In the evaporator, the refrigerant is turned into gas form, which absorbs heat and thus cools the surroundings. The colder air is transferred with a fan to the desired location. The gas refrigerant then returns to the compressor (4) and the cycle repeats. The pressure difference in (1) and (4) corresponds to the work added on the compressor. In a bus this would correspond to taking hot air from outside of the bus, cooling it with the motor as a power source and distributing cold air through the air-conditioning channel to different areas inside the bus.

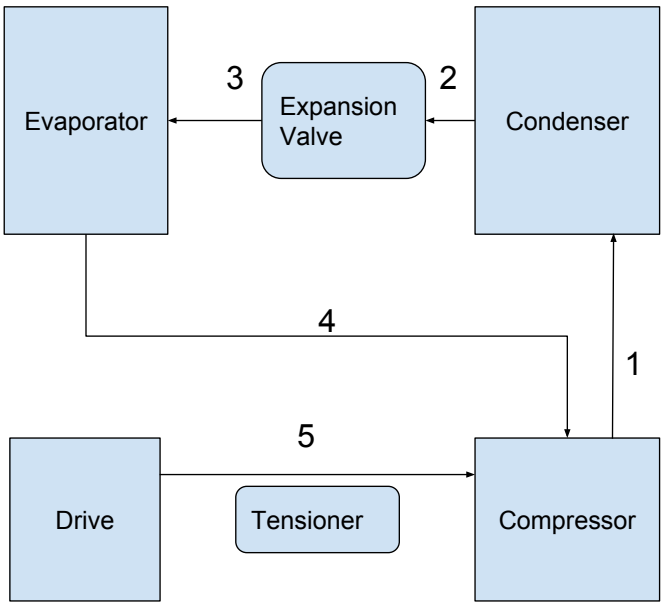

Figure 2.1: Simplified schematic sketch over a compressor driven air-conditioning system powered by a motor with a drive belt. (1) gas/high pressure, (2),(3) liquid, (4) gas/low pressure, (5) drive system.

2.3 Maintenance

The theory about maintenance can be divided into four different levels; reactive/corrective, preventive, predictive and proactive which has gradually developed since the beginning of the industrial era. Reactive or corrective maintenance is considered to be when products are used until a failure occur. Once the failure has happened, the product is repaired or replaced with new parts. This was a viable strategy for a long time but with increased complexity in machinery, the possible profit of decreasing down times have led to new strategies.
One way is to use preventive maintenance, i.e to use measures that extends the life span of a product. A common implementation of this methodology is to periodically schedule maintenance whether it's needed or not. The negative side with preventive maintenance is that some parts may be maintained even if the conditions are good or that failure may occur before the product could be maintained. The procedure

rarely takes into account how the product is used or how different environmental conditions may lead to premature failures. One of these preventive measures could be to periodically add grease to a gear.
Predictive maintenance (PM) aims to reduce downtime and maintenance by monitoring different conditions, giving an alarm before something is about to go wrong. Basic examples are when the oil level in a car is to low or when the performance of a system is lower than expected.
Where PM looks at the symptoms in a system, a further development of the maintenance is to use Proactive maintenance that aims to diagnose a symptom and to find the underlying problem behind it.
Belt drives are failing due to a number of different reasons. According to [1], 42% of the failures in belt drives are due to that parts are not maintained when they should be, furthermore 20% are due to improper installation. By detecting these two components, it would be possible to schedule maintenance before a breakdown or to redo the installation before it causes more damage to the system. While improper maintenance eventually leads to a low tensioned belt drive, improper installation might be a belt that is initially too high or low tensioned.
Predicting the symptoms of these problems could therefore reduce belt drive break downs with up to 62% and greatly decreasing the maintenance cost. In the Figure 2.2, a diagram illustrates the causes of the most common failures.

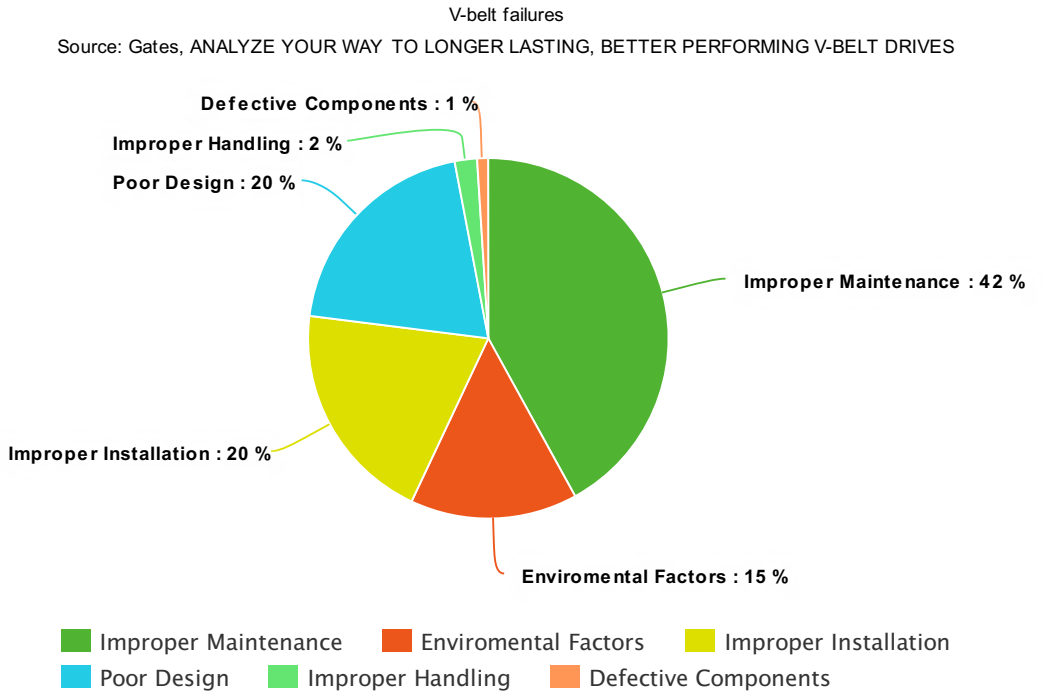

Figure 2.2: Failure causes in belt driven systems. Problems caused by ill maintained belts and improper installation amounts to 62% according to [1]. Figure used with permission from Gates Corporation.

Conducting maintenance with perfect timing is a matter of economizing and using earth's limited resources in an optimal way. Decreasing the amount of unnecessary

belt changes is not alone going to make any significant difference on a global scale, but it hopefully works as a case showing how modern sensors, connectivity and algorithms can be used towards a more sustainable and resource-conscious society.

2.4 Analysis of the system

There are mainly three factors considered here that are expected to be closely related to belt tension; belt slip, heat development from friction between belt and pulley surface and belt vibrations. These factors will be observed with a set of sensors, some are of expensive high-performance type and may be used as a way to correlate and eventually verify what can be interpreted from the less expensive, closer to production-grade, sensors. The following section describes how these three factors is related to the overall goal of determining belt tension.

2.4.1 Belt slip

Belt slip is the term used here to describe two or more pulleys connected with a power transmission belt that are rotating with varying transmission ratio, i.e the belt loses traction with the pulley surface and hence they will rotate with different speeds until traction is restored. Belt slip occurs when the torque in a pulley is large enough to overcome the static friction force acting between belt and pulley surface. Belt slip is gradual and it begins where the belt exits the pulley. The slip angle β can be defined as the angle of the arc on the pulley surface where belt slip has begun, with slip angle = 0 ° being no slip and then increasing until the slip region covers the entire contact surface between belt and pulley, then full slip is achieved. Figure 2.3 shows a graphical description of the phenomenon. An simple analytic approximation of the belt slip angle can be expressed as

$$\beta = \frac{1}{\mu} \ln \left(\frac{T_t - Gr\omega}{T_s - Gr\omega} \right) \tag{2.1}$$

where μ is the friction coefficient between the surfaces, r is the pulley radius, G is mass flow per second of a belt, ω is rotational speed and T_t and T_s are the belt tension in N on the tight and slack side of the belt, respectively [7].

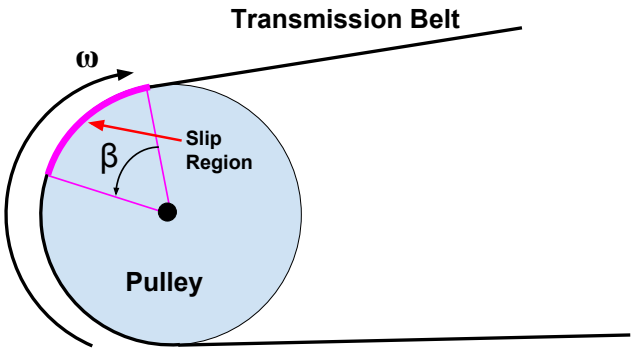

Figure 2.3: Simple schematic showing how belt slip develops. β is the slip angle and ω represents the rotational speed of the pulley.

2.4.2 Temperatures

To connect belt tension with observed heat development, a very simple generic model is developed. The goal is to achieve a model where tension is a function of things that can be measured and a few physical and geometrical parameters that can be estimated one time when the belt is installed and the tension can be considered as known. By assuming that the material- and geometrical properties are constant over the belts life time, the model should then be able to solve for the unknown tension at any given point in the future. The temperature of the system depends on heat transferred by convection, conduction or radiation where the main sources affecting the belts are expected to be

- Ambient air temperature
- Heat generated from friction in bearings
- Heat developed from the bending of the belts
- Heat developed from friction between belts and pulleys
- Radiation from warm objects.

The ambient temperature is affecting belts and components through convection where the air removes heat from the system. The temperatures of the pulleys will transfer heat through physical contact (conduction). When belts are being bent at the pulleys and straightened out, heat will develop due to inner friction (hysteresis) in the belt. When slip occurs, due to insufficient tension or rapid change of load, heat will develop from the friction between the two components. Warm objects in the surroundings, like the motor or compressor may radiate heat and effect the system.
A way to model the frictional moment, M, in bearings has been developed by *SKF* [8] and results in the power loss

$$P_{\text{loss}} = 1.05 \cdot 10^4 Mv \tag{2.2}$$

where v is the rotational speed. The frictional moment in the *SKF* model depends on many parameters related to bearing type or lubricant but it is also dependent and forces applied to the bearing. Since the radial force on the bearing would increase with higher tension it could be possible to reformulate a simplified function where the heat generated in the system is directly dependent on the tension of a belt.
A simple function of the changes in temperature in a part of the system could then be formulated as

$$\dot{T} = f(T, T_{\text{air}}, v_{\text{drive}}, F_{\text{belt}}) \tag{2.3}$$

where T is the temperature, T_{air} is the ambient temperature, v_{drive} is the motor speed and F_{belt} is the tension in the belt. To simplify, the radiation from warm objects and the conduction from the other components are omitted. The temperature in a part of the system would be stable when the heat developed dependent on speed, temperature difference and tension sums to zero. Some material constants would have to be measured or estimated from a real system or taken from component specifications. It could also be done on a physical test rig or by measuring the temperature and then tune the parameters to match the temperature measurements. The parameter estimation could also be solved as a minimization problem, where measurements are used to fit the model.
With a model that sufficiently describes the temperature changes it is possible to solve the equation for tension, obtaining a model where tension can be estimated using temperature and speed measurements.
The the heat generating contribution could then be set up as

$$H_{\text{tension}}(t) = c_{\text{tension}} \cdot F_{\text{belt}} \cdot v_{\text{drive}}(t)^{c_{\text{v}}} \tag{2.4}$$

and cooling of the system as

$$C_{\text{air}}(t) = c_{\text{air}} \cdot (T(t) - T_{\text{air}}(t)) \tag{2.5}$$

where c_{air} is a constant dependent on the surface area and the conductivity of the body, c_{tension} is a constant dependent on how much the tension affects the system and c_{v} an unknown factor for the speed.
By assuming that (2.4) and (2.5) contributes most to the temperature difference gives

$$\dot{T}(t) = H_{\text{tension}}(t) - C_{\text{air}}(t) \tag{2.6}$$

and solving for belt tension, F_{belt}, results in

$$F_{\text{belt}} = \frac{\dot{T}(t) - c_{\text{air}} \cdot (T(t) - T_{\text{air}}(t))}{c_{\text{tension}} \cdot v_{\text{drive}}^{c_v}} \tag{2.7}$$

where T, T_{air} and v_{drive} needs to be measured online and the constants c_{v}, c_{air}, and c_{tension} needs to be estimated.
The parameter estimation can be done with a nonlinear least-squares solver which solves the minimization problem

$$\min_x ||f(x)||_2^2 = \min_x (f_1(x)^2 + f_2(x)^2 + ... + f_n(x)^2) \tag{2.8}$$

where $f_i(x)$ is the difference between the measurement $\dot{T}$(t) and the model in Equation 2.6 and x is a vector with the parameters c_{v}, c_{air}, and c_{tension}.

2.4.3 Vibration analysis

The vibrations from rotating machinery can be very informative and to exploit the information embedded in the vibrations the Discrete Fourier Transform(DFT) works as a very powerful tool.
The system under investigation is expected to exhibit several vibration components originating from different sources and causes. It is highly likely that the vibrations from the motor or the compressor will propagate through the belts and the construction. Furthermore, if any of the rotating bodies in a transmission system have an imperfection such as eccentricity, they will produce a vibration at the fundamental rotation frequency and possible higher harmonics.
The intention with this work is however to find vibrations related to the tension level in the belt. Everyone knows how the tone (frequency) changes in a guitar string when varying the tension with the tuning pegs. A widely used way to describe power transmission belts is called the string model and it stems from the assumption that the belt can fundamentally be described as a simple vibrating string. Here the vibrations in a moving belt is of interest and the position of the transverse wave in a moving belt can be described as

$$v(x,t) = \sin\left(\frac{n\pi x}{L}\right) \cdot \sin\left(\frac{|c^2 - V^2|T + Vx}{cL}\right) \tag{2.9}$$

where x is the position along a belt with a span L m between two pulleys, n is the wave's harmonic order, V is the speed of the belt expressed in m/s, T is the tension in N and c is the speed of the transverse wave in m/s. The speed c can be expressed as

$$c = \sqrt{\frac{T + \eta m V^2}{m}} \tag{2.10}$$

with m corresponding to the belt's mass per meter and η being a constant between zero and one, representing the stiffness of belt relative to the pulley mounting, where $\eta = 1$ corresponds to a belt as stiff as the mounting itself. The fundamental frequency of the transverse wave can be expressed as

$$f = \frac{c^2 - V^2}{2Lc} \tag{2.11}$$

From these relationships, it is clear that the belt's vibration is dependent on speed and tension [3]. Equation 2.11 can be used to locate vibration components that are immediately connected with the transverse waves in the belt and in that fashion determine the belts tension.

2.4.4 Statistics

Plenty of previous work in the field describes how kurtosis of signals can be used to determine the condition and detect abnormal behaviour, especially in rotating machinery.

Kurtosis is the fourth standardized moment of a probability distribution and is defined as

$$k = \frac{E\Big[X - \mu\Big]^4}{\sigma^4} \tag{2.12}$$

where X is the random variable, μ is its mean value, σ its standard deviation and $E\Big[\ \cdot\ \Big]$ is the expected value.
The standard use of kurtosis is as a measurement of how prone a given statistical distribution or process is to extreme values. Values of X further away than one standard deviation will make a larger contribution, hence this metric is used as a tool to detect outliers in data. Another common way of using kurtosis is as a measure of heaviness or peakedness of the underlying distribution, since more observations far away from the mean will result in more mass in the tails of the distribution and the opposite will give a more distinct peak, i.e a way to quantify the shape, this is however not the correct interpretation of the kurtosis.
The standard normal distribution has a kurtosis value of 3 and larger values corresponds to more observations far from mean, called *leptokurtic* and the opposite, a value less than 3, is named *platykurtic*. The benefit of using kurtosis when monitoring machinery is that it can help detect the presence of occasional irregulareties during operations, the value can be calculated instantaneously and then compared over time.
In [9] it is showed that by looking at the kurtosis of the vibrations picked up by seismic sensors, it is possible to discriminate the footsteps of a person walking from other sources of ground vibrations, for example motor traffic, because of the impulsive nature of the source. An analogy to the work focused on here is that intuitively a loose belt should exhibit a more impulsive behaviour because the slack increases the possibility of belt flapping, while a well tensioned belt will be firmly kept in place.

3
Methods

This chapter deals with how the work was carried out to solve the problem under investigation. Here follows descriptions of how the experimental data was collected and filtered, how the experiments were conducted and what instruments were used.

3.1 Design of test rig

For the purpose of collecting realistic data a test rig was designed and constructed. The test rig was designed with the intention to resemble an air conditioning (AC) system that can be found in a bus. The compressor belt is the main part under investigation and the simplest test rig could consist of just a motor driving a pulley with a static load with a belt power transmission. This is indeed how a lot of previous research have been conducted, with a small scale power transmission, relatively low load and belt tension. To capture more of the dynamics of a real system, the test rig constructed here comprise a production type compressor with a suitable motor and also the entire AC system with evaporator and condenser. This setup will give more realistic working conditions when it comes to vibrations and heat transfer.

3.2 Setup

This section describes the test rig and its specifications with the most relevant components.

3.2.1 The test rig

The compressor chosen was a Bitzer 6NFC reciprocal compressor driven by a 20hp Baldor electric motor. A conventional bus usually uses a diesel engine but since it is both cheaper and easier to operate an electrical motor the latter was used in the setup. The motor was connected by two separate belts with the compressor via an intermediate idle pulley suspended by the so called tension arm. The physical dimensions of the pulleys and belts are displayed in table 3.1. The electric motor was controlled with a variable frequency drive (VFD) that lets the operator set a nominal motor speed in steps of 30 RPM from 0 to 1800. The compressor pulley was connected with the compressor itself via a magnetic clutch and a separate power supply could then be used to energize the clutch, thus engaging the compressor. Fans were mounted on the evaporator and condenser to control the process, by adjusting the fan speed it's possible control the temperature of the conditioned air and the

compressor discharge pressure. The latter is of most interest here, since the pressure was used when defining the load.

Part	Dimension
Motor pulley radius, r_m	123 [mm]
Tensioner pulley radius, r_t	101.6 [mm]
Compressor pulley radius, r_c	103 [mm]
Drive side belt length, L_d	1600 [mm]
Compressor side belt length, L_c	1270 [mm]

Table 3.1: The physical dimensions of pulleys and belts.

Figure 3.1 displays the complete test rig and the most important parts are highlighted, the total weight of the rig is > 500 kg, which gives an idea of the proportions. To the left is an electrical motor, in the middle the tension arm and to the right the compressor. A condenser is placed on the steel frame with an evaporator mounted on top of it. On the trolley to the right are both the VFD and the power supply for the magnetic induction clutch on the compressor. Figure 3.3 gives a more detailed view of motor, compressor and sensor positions.

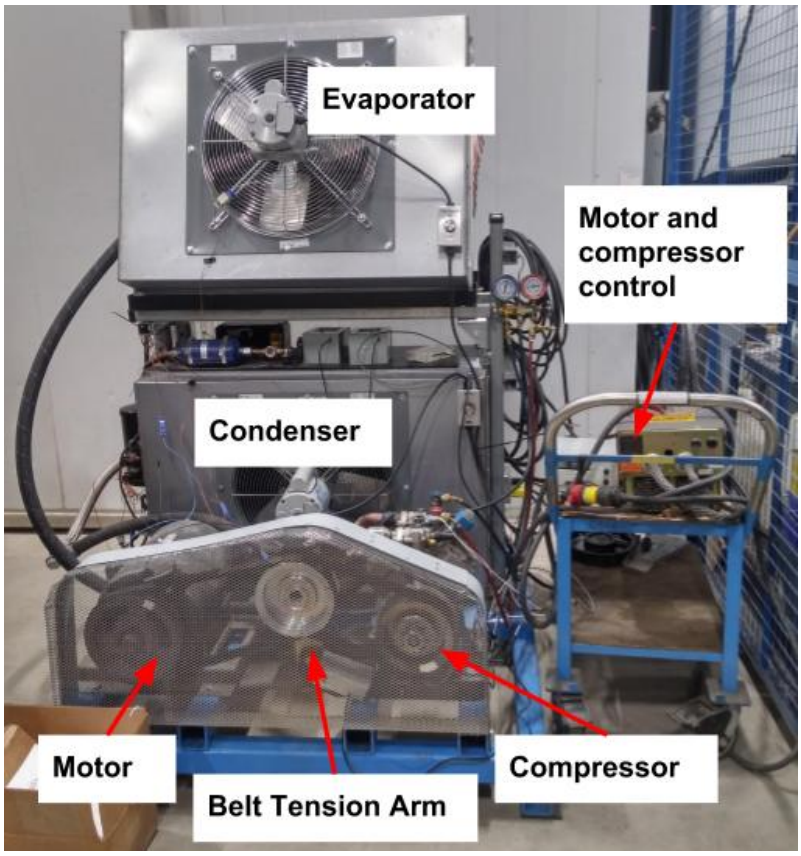

Figure 3.1: The test rig that was constructed to perform the tests.

3.2.2 Tension arm

The tension of the compressor belt can be relatively easy adjusted by a technician thanks to the MCC patented belt tension arm, see Figure 3.2. The tension arm is a mechanical construction that is mounted on an axle on the same base plate as the compressor, allowing it to rotate along the direction the belt is running. The shaft of the pulley on the tension arm is fixed inside a brass block which in turn is suspended with a screw, turning the screw makes the pulley move up or down thus increasing the distance between the centers of the three pulleys. Since the arm is free to rotate along the belt, it will always be positioned in an angle where static force equilibrium is achieved. Due to the length of the belts and position of the arm, the tension in the shorter belt on the compressor side will be slightly higher than in the belt on the motor side.

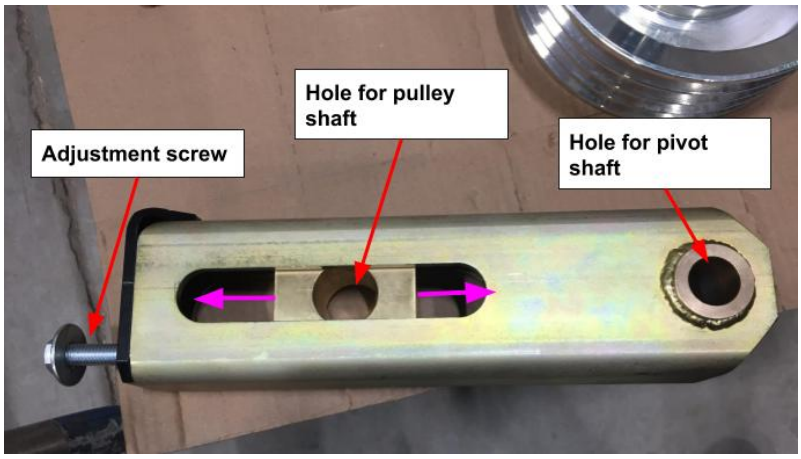

Figure 3.2: The tension arm before it's assembled. In assembled state it will rest on a shaft going through the hole on the right hand side in the picture. The idle pulley(or the tension pulley) will be suspended in the block by a shaft through the other hole, making it possible to adjust the height and thus the tension with the screw.

3.3 Sensors

The sensors were chosen to ensure that the conditions of interest could be measured, i.e temperature caused by friction in the belt, rotational speed of the pulleys and vibrations in the belt. To capture the state of the AC system, thermocouples were placed at key locations on the test rig, i.e the evaporator and condenser air coming in and out, the refrigerant temperature going in and out of the evaporator and also the temperature of the refrigerant going in to the condenser. To being able to monitor the compressor load a pressure sensor was added to the compressor measuring the pressure on both sides, suction and discharge pressure. Signals from the VFD were also extracted, especially the motor current, to see how the motor torque changes. From the VFD was also the motor voltage readily available.

3.3.1 Photoelectric sensor

The photoelectric sensors were used to measure the rotational speed of the motor and compressor pulleys. It works in such a way that an optical amplifier counts the number of times it detects a reflecting reference points (e.g pieces of reflective tape) attached on the rotating surface within a specific time window. The frequency at which the reference points are detected is then converted to a voltage proportional to the rotational speed in *revolutions per minute* (RPM). The optical amplifier used was an *Automation Direct DFP-AP-1A* and the frequency converter was a *Red Lion IFMA0035*. The rotating pulleys were equipped with two pieces of reflecting tape each, placed 180° apart facing the direction perpendicular to their rotation. With maximum motor speed being 1800 RPM the maximum frequency at which the reflective tapes can be detected equals $\frac{2 \cdot 1800}{60} = 60$ Hz. The speed transmission ratio from motor to compressor is approximately 1.25, giving a corresponding maximum frequency of 75Hz. Based on this and some extra margin, the frequency range were set to 80 Hz for the motor and 100Hz for the frequency converter on the compressor side, i.e maximum voltage output from the converter would then represent 80 or 100 Hz. The time window during which the frequency is calculated is called the minimum response time, on the motor side it was to 500 ms, which means that at 800 RPM the sensor will observe 13 negative edges and calculate the average frequency during that time. On the compressor side the minimum response time was set to 200 ms, which at 800 RPM on the motor (lowest intended speed and thus worst case) gives 6 negative edges. This is a classic trade off between time and frequency resolution, longer time window will give more accurate speed measurements but will be worse at detecting sudden speed changes.

3.3.2 Infrared thermocouples

Two infrared thermocouples were used for contactless measurement of surface temperatures by measuring thermal radiation from the belts. One was placed on the compressors side and the other on the motor side. According to the theory stated earlier, belt slip is expected to occur first in the region where the belt leaves the pulley. In this case, having a clockwise belt rotation, the belt will exit the pulleys above the motor and below the compressor, respectively, and that is where the thermocouples were placed, to capture temperature increases due to slip. One could argue that the thermal inertia of the belt makes the sensors' positions irrelevant, but since the belt is exposed to cooler and streaming air almost half the time it is reasonable to expect local differences in temperatures, however small they might be. This set-up should at least provide similar conditions for the two sensors.

3.3.3 Surface thermocouple

On the shaft of the tensioner pulley a surface thermocouple was placed to monitor how heat in the bearings develop.

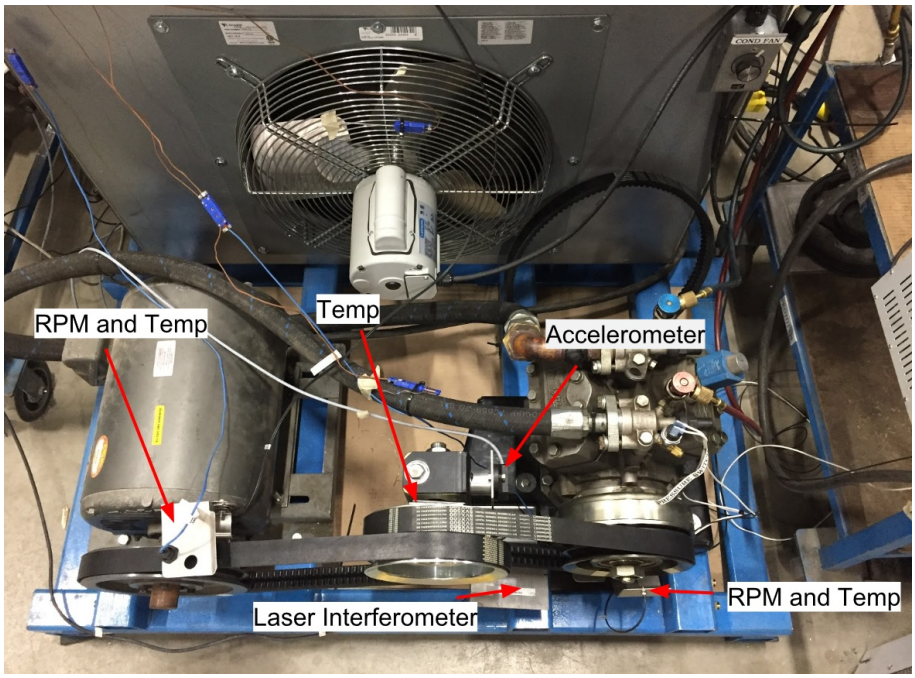

Figure 3.3: A more detailed view of the test rig, showing the motor, compressor, tension arm and some of the most important sensors.

3.3.4 Accelerometer

An accelerometer was placed on the upper right side of the tension arm, to monitor the vibrations acting upon it. The sensor measures acceleration in three directions, with the X-axis upwards along the tension arm, the Y-axis pointing out from the test rig, perpendicular to the belts' extension and the Z-direction is being along the belt.

3.3.5 Laser interferometer

A laser interferometer was added to measure the vertical movement of the belt, the vibrations in it. The sensor was mostly added to be used as a reference for the tests and is not realistic in a real situation due to its high cost and intolerance towards such harsh environment.

3.4 Procedures

The following section describes how the experiments were conducted and which parameters that were changed.

3.4.1 Tension measurement

While it is difficult to measure belt tension when a machine is running, it's rather easy to do when the machine is stopped. To get the initial tension for all the tests, a Sonic Belt Tension Meter 508C from *Gates* was used. The instrument

basically measures the fundamental frequency of a belt by assuming that the law of vibrating strings can be applied. By pushing down the belt it starts to vibrate, like the vibration from hitting a guitar string. The sensor picks up the sound from the vibrating belt and determines the fundamental frequency. By entering system parameters it is then possible to determine tension from

$$T = 4MWS^2f^2 \cdot 10^{-9} \tag{3.1}$$

where T is the estimated tension in N, M is a mass constant in g/m depending on the belt model used, W is the number of strands that the belt has, S is the distance in mm of the free span of the belt and f is the fundamental frequency in Hz estimated by the meter. The free span can either be measured from the points where the belt leaves the pulley, or calculated from

$$S = \sqrt{C^2 - \frac{(D_1 - D_2)^2}{4}} \tag{3.2}$$

where C is the distance in mm between the center of the pulleys and can easily be measured and D_1 and D_2 are the diameters of the pulleys in mm. Since there is an uncertainty in the frequency measurements, the indicated tension fluctuates a bit, thus several measurements were taken to get the best estimate of the belt tension, this is also in accordance with the manufacturer's recommendation. Another circumstance that further adds uncertainty to the measurements is the fact that the two belts are suspended in three different sized pulleys. Ideally this would not affect the tension at any one point in the belt, however in reality each pulley and its shaft mountings have non-idealities such as eccentricity and miss alignment. These defects might not be visible to the naked eye but when turning the pulleys it will introduce tension variations in the belt as the distance between the outermost points of the belt's suspension varies. Table 3.2 summarizes the recommendations made by an experienced technician, when it comes to tightening a 2 strand power V-belt. The original recommendations were made in the imperial units of pound-force (1 lbf = 4.445 N), which is the accepted unit in the trade.

Belt tension		Classification
>300 lbf	= 1334 N	Dangerously high
≈ 180 lbf	= 800 N	Recommended
<100 lbf	= 444.8 N	Dangerously low

Table 3.2: An overview of belt tension recommendations made by an experienced technician.

The measurements were always taken on the longer of the two belts because the span on the short belt is very close to the minimum span that the belt tension meter can make reliable measurements.

3.4.2 Parameter space

There are mainly three factors that will be varied in different combinations; belt tension, motor speed and load. To keep the number of different experiments within

a feasible range, the number of levels were kept at a minimum for speed and load to allow for higher resolution in the belt tension parameter. Initial test parameter considerations also included ambient temperature and belt angle but these were later rejected to keep the complexity down. Belt tension, speed and load should be sufficient as variable parameters to find general signs of a belt in need of maintenance. The motor speed levels chosen were 800 RPM, 1200 RPM and 1600 RPM, where 800 corresponds to an idling diesel engine in a bus, 1600 is roughly the highest motor speed in normal operations and 1200 is somewhere in between. Since the VFD only allows the speed to be set in integer multiples of 30, the nominal speeds were 810 RPM, 1200 RPM and 1590 RPM. The actual speed will typically be a little bit lower and fluctuating, especially with higher loads.
As explained before, belt tension measurements are affected by relatively high uncertainty, therefore instead of trying to determine belt tension to the exact number, tension levels were divided into four groups where category C is the desired level. The groups are defined in table

Group	A	B	C	D
Belt tension [lbf]	65-85	100-150	180-200	270-310

Table 3.3: Definition of belt tension groups.

The load was also divided into separate groups, high load, low load and no load. The subsequent grouping of load is found in table 3.4.

Nominal speed [RPM]	810	1200	1600
High load	4.4-5.0	5.8-6.0	7.0-7.1
Low load	3.5-3.7	4.50-4.55	5.7-6.0
No load	1	1	1

Table 3.4: Definition of compressor load levels.

The load was quantified as

$$Load = \begin{cases} \frac{PSI_{Discharge}+14.7}{PSI_{Suction}+14.7}, & \text{if Compressor=On} \\ 1, & \text{if Compressor=Off} \end{cases} \tag{3.3}$$

where 14.7 PSI is the the atmospheric pressure. The load was controlled by adjusting the speed on the evaporator fan, full speed resulted in the lowest discharge pressure and lower speed increased pressure. The condenser fan speed was always kept constant at full speed. According to the supervising system specialist, the recommended discharge pressure is in the range 150-300 PSI (1034-2068 kPa). Since the discharge pressure also depends on the motor speed, the two load levels were defined differently for each nominal speed, based on what discharge pressure could be achieved at a certain speed. The defined load regions vary in width because of difficulties of sustaining an exact pressure over time, except fan and motor speed the pressure was also affected by ambient temperature and a flow regulator in the coolant tubing, factors that could not be controlled.

Factor	Belt tension [N]	Motor speed [RPM]	Load [-]
Levels	133-1334	810,1200,1590	No, Low, High

Table 3.5: The main factors that was varied in the experiments and their levels.

Each new test session started with approximately 15 minutes warm up, where the system was just run at an arbitrary speed (within the 800-1600 range) and with or without load, before it was stopped and the tension was measured and adjusted, if needed. Then each specific experiment began with ramping up the motor to reach steady speed at desired level, which occurred almost in the same instant as the speed was set. Then the two fans (evaporator and condenser) were engaged at full speed and the compressor clutch energized, resulting in a reduced speed which within a few seconds settled at a level up to 30 RPM lower than nominal speed. At this point the evaporator fan speed was manipulated to change the load, i.e the discharge pressure. To achieve higher load, the fan speed was decreased by simultaneously observing the pressure until steady state at desired level was reached. This kind of manual control towards a desired value could sometimes be time consuming, therefore the fan speed was measured and noted when the pressure had reached steady state in order to improve the repeatability and more quickly get to desired load. Those measurements were done with the belt tension meter, by directing the sensor towards the tip of the rotating fan blades their frequency was obtained and the rotating speed could then easily be calculated by multiplying the frequency with 60s and divide with 3 (fan blades) to get speed in RPM. With steady discharge pressure the system was left running at least 120 seconds (sometimes longer) to collect enough data in steady state for the subsequent analysis. All sensor values were collected from the moment the motor was started to its termination, allowing for analysis of both steady state and transients.

The observed parameters (Table 3.6) shows the measurements that were taken during the data collection process.

Low frequency		High frequency	
Factor	Unit	Factor	Unit
Motor rotation	RPM	Belt displacement	mm
Compressor rotation	RPM	Tension arm acceleration, X	g
Belt surface temperature, motor side	°C	Tension arm acceleration, Y	g
Belt surface temperature, compressor side	°C	Tension arm acceleration, Z	g
Tension arm pulley surface temperature	°C		
Evaporator air out temperature	°C		
Evaporator air in temperature	°C		
Condensor air out temperature	°C		
Condensor air in temperature	°C		
Evaporator refrigerant out temperature	°C		
Evaporator refrigerant in temperature	°C		
Condensor refrigerant in temperature	°C		
Compressor suction pressure	PSI		
Compressor discharge pressure	PSI		
Motor voltage	$Volt$		
Motor current	$Ampere$		

Table 3.6: Observed parameters during the test process.

3.5 Conducted experiments

Table 3.7 summarizes the experiments conducted according to the before mentioned procedures.

3.6 Data analysis and processing

This section describes how the collected data was used and how the signals were processed. Since there is no way to know with absolute certainty the true speed or true temperatures, the goal with the filtering here was to remove apparent outliers and get rid of variations in the signal that was clearly unlikely considering the dynamics it was capturing while still tracking quick step changes.

3.6.1 Speed

The collected signals from the speed sensors contained a high amount of outliers and rapid changes that can be regarded as noise coming from the sensor itself, the frequency converter and/or the (data acquisition) DAQ instrument, see Figure 3.4 for the unfiltered signals. The first step in filtering of theses two signals (motor speed and compressor speed) was to remove apparent outliers, it was implemented with MATLAB's Hampel filter. The Hample filter runs through the collected signal and for each sample it calculates the standard deviation from the mean based on the $\pm n$ adjacent samples. If the value of the current sample is larger than three standard

Test	Tension [lbf]	Tension category	load [-]	Load group	Nom. speed [RPM]
A1	75	A	5,00	high	810
A2	85	A	3,70	low	810
A3	85	A	0,00	no	810
A4	70	A	5,80	high	1200
A5	65	A	4,50	low	1200
A6	70	A	0,00	no	1200
A7	85	A	7,00	high	1590
A8	85	A	5,70	low	1590
A9	75	A	0,00	no	1590
B1	100	B	4,40	high	810
B2	150	B	3,50	low	810
B3	125	B	0,00	no	810
B4	110	B	5,80	high	1200
B5	140	B	4,55	low	1200
B6	140	B	0,00	no	1200
B7	150	B	7,00	high	1590
B8	150	B	6,00	low	1590
B9	100	B	0,00	no	1590
C1	180	C	4,50	high	810
C2	180	C	3,70	low	810
C3	180	C	0,00	no	810
C4	190	C	6,00	high	1200
C5	195	C	4,55	low	1200
C6	190	C	0,00	no	1200
C7	180	C	7,00	high	1590
C8	180	C	5,70	low	1590
C9	180	C	0,00	no	1590
D1	300	D	4,50	high	810
D2	310	D	3,70	low	810
D3	310	D	0,00	no	810
D4	270	D	6,00	high	1200
D5	310	D	4,50	low	1200
D6	270	D	0,00	no	1200
D7	310	D	7,10	high	1590
D8	310	D	5,70	low	1590
D9	310	D	0,00	no	1590

Table 3.7: Detailed list of all test, according to the explained test plan.

deviations, it is replaced with the mean value. The observed outliers tend to consist of only one sample, hence the number n can be chosen fairly small, MATLAB default is $n = 3$ for example. Figure 3.5 shows the difference between Hample filters with $n = 3$ and $n = 15$.

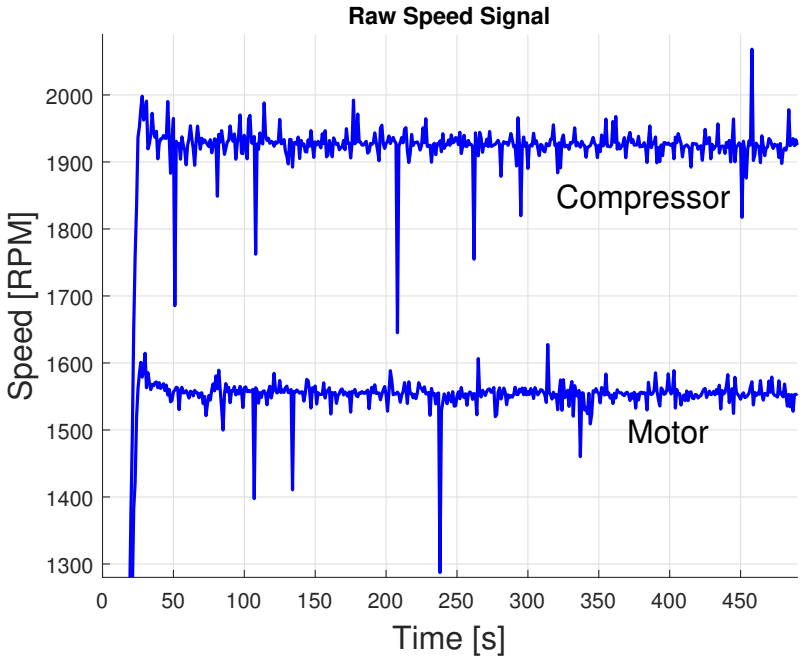

Figure 3.4: The raw speed signal from motor and compressor shows the existence of multiple outliers. The data comes from operating point C7.

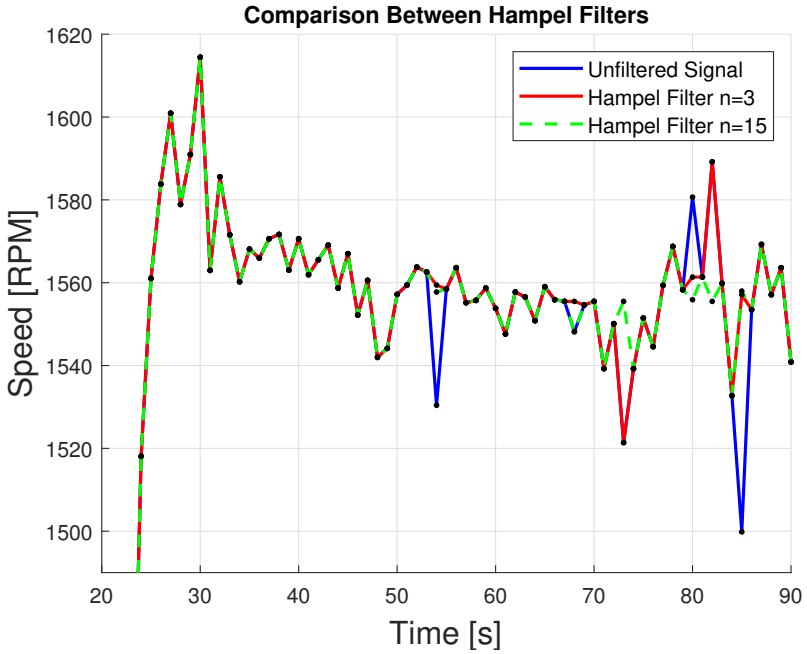

Figure 3.5: A comparison between two outlier filters of type Hampel. It shows the effectiveness of the Hampel filter with $n = 3$ (red) and $n = 15$ (dotted green), compared to the original (blue) signal.

With outliers removed there were still some higher frequency noise present, visible as unlikely quick speed changes, the 50 RPM speed drop in one second observed after 30 s in Figure 3.6 for example. Two methods were considered to remove these high fluctuations, a simple moving mean and more sophisticated Butterworth low-pass filter (LPF). The Butterworth filter was chosen since it has a flat amplitude response in the pass band, compared to other filters that may exhibit ripple characteristics in the pass band. The trade-off is a wider transition band, i.e other filters may be better at removing frequencies close to the desired pass band. More details about the Butterworth filter can be found in [10]. In this work the filter was implemented using MATLAB's filter design function *butter*. Figure 3.6 shows the signal with outliers removed together with three different window sizes of moving mean filtered signal and one signal filtered with a 9th order Butterworh LPF with cutoff frequency equal to 0.05 Hz. It is clear that the LP filtered signal shows the most probable trajectory of the speed signal, following the Hampel filtered signal closely during the initial speed ramp and it is not affected with rapid sample-to-sample variations.

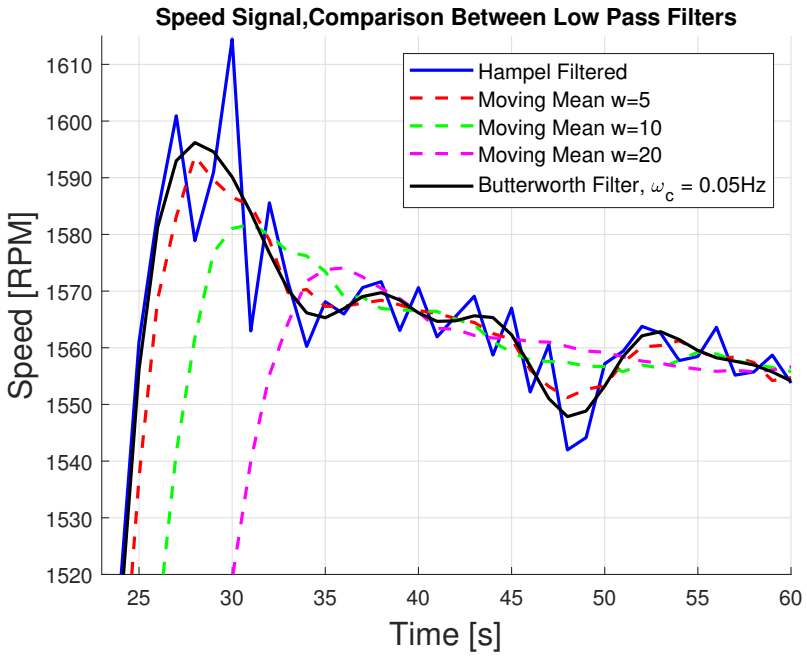

Figure 3.6: A comparison between low-pass filters. The filtered signal have already had its outliers removed (blue signal), with a Hampel filter. The moving mean filters differ in window size w, within which the mean is calculated.

3.6.2 Temperature

Figure 3.7 shows the unfiltered temperature signal captured from the infrared thermocouple at the drive belt and the surface thermocouple at the tensioner pulley shaft. These signals does not seem to have any apparent outliers but shows some high frequency variations which are much faster than the temperature dynamics and hence considered as unwanted noise.

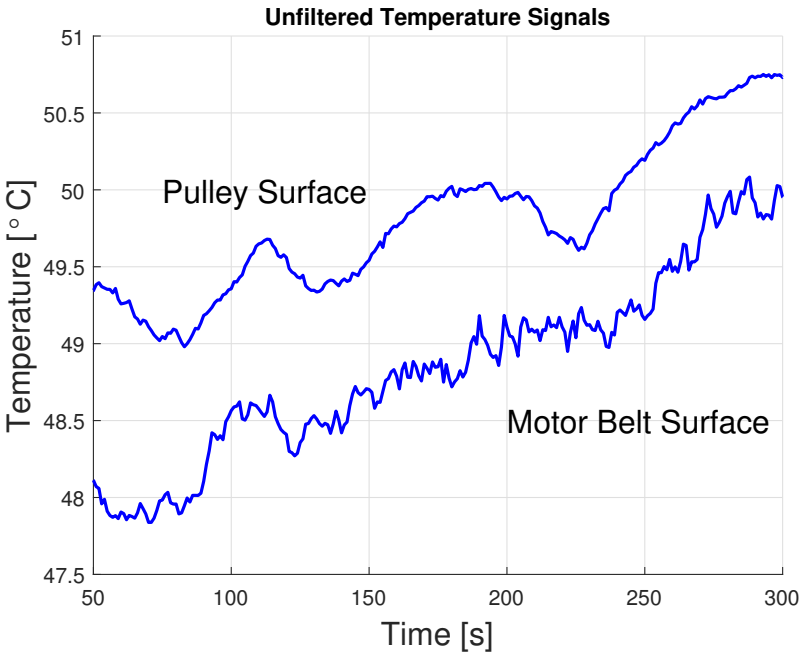

Figure 3.7: Unfiltered temperature data. Surface temperature from infrared thermocouple on the drive belt and surface temperature from surface themorcouple on the tensioner pulley shaft.

The filtering of the speed signals in the previous section showed that a Butterworth LPF was an efficient method to get rid of quick fluctuations and therefore the same filter was here applied and Figure 3.8 and Figure 3.9 shows the result from using two different cutoff frequencies.

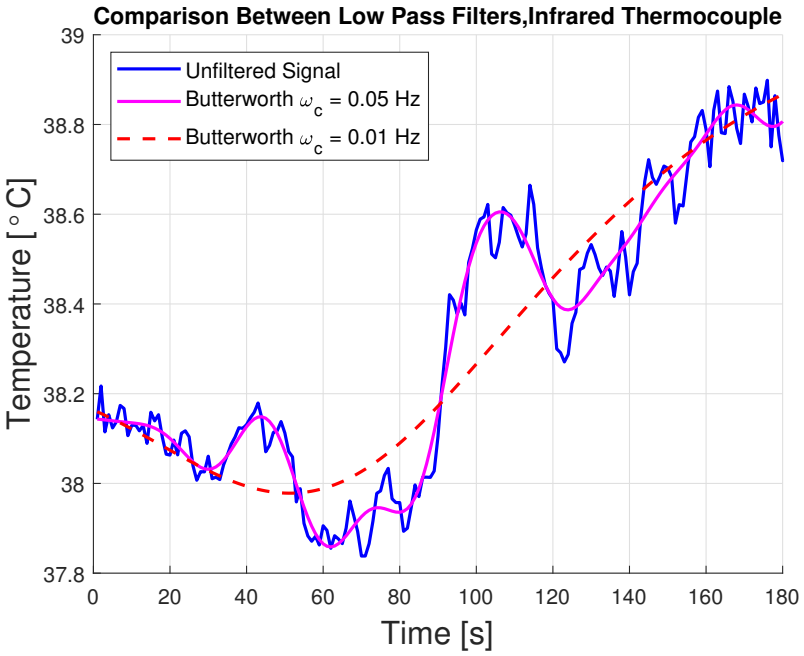

Figure 3.8: Infrared thermocouple temperature signal filtered with a Butterworth low-pass filter with two different cutoff frequencies, compared to the unfiltered signal.

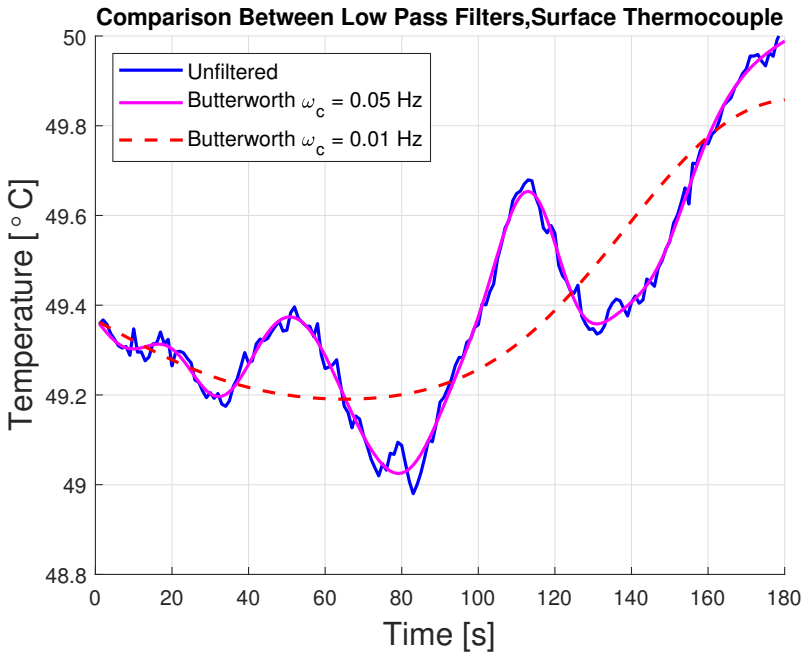

Figure 3.9: Surface thermocouple temperature signal filtered with a Butterworth low-pass filter with two different cutoff frequencies.

The infrared sensor contains a bit more noise, which is reasonable since the surface which it's observing is constantly moving. Out of two filters the one with cutoff frequency equal to 0.05 Hz gives the most reasonable result in both cases. The resulting filter was then also applied to the infrared thermocouple on the driven compressor belt.

3.6.3 Pressure

The pressure signal was filtered with the same reasoning as was used for the speed and temperature signals, first removing outliers and then applying a LPF to get a reasonable result considering the dynamics of the measured quantity. Figure 3.10 shows the unfiltered discharge pressure signal together with LP-filtered signals using the same 9th order Butterworth filter also used in the previous two sections.

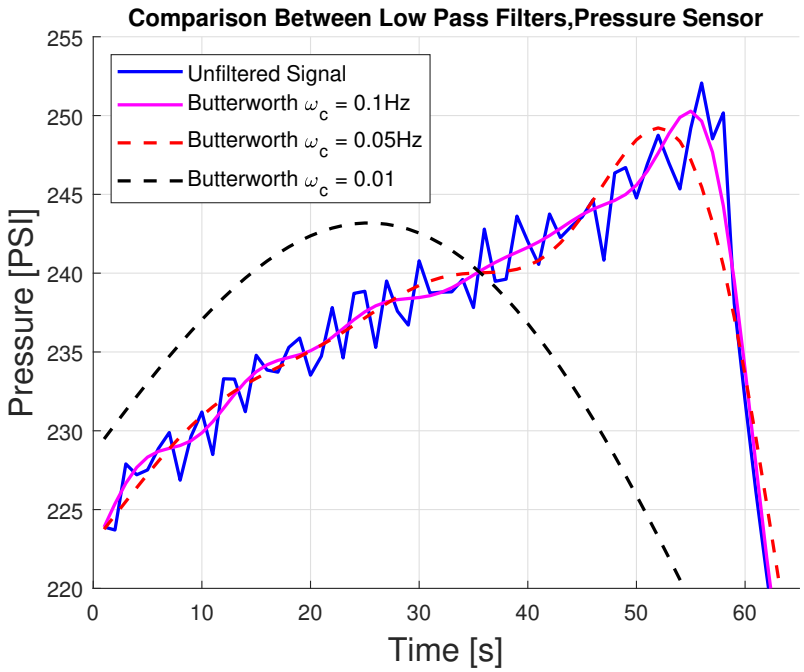

Figure 3.10: Unfiltered discharge pressure signal (blue) together with Butterwoth low-pass filtered signal with three different cutoff frequencies.

Based on this result, the LPF with 0.1 Hz cutoff frequency was chosen since it filter out the small (only about ±2% of the LP filtered signal) fluctuations and still shows a quick response to the sudden pressure drop in the end of the captured signal above. It is of course hard to definitely tell whether these pressure fluctuations observed every second are reasonable or not, on the other hand is it of no interest to know if the pressure changes a few PSI every second, the important information is the more slowly changing pressure level since the load is defined as an average fraction of discharge to suction pressure. The same filter was then also applied on the suction pressure signal.

3.6.4 Accelerometer

To test the accelerometer's performance it was exposed to the worst case vibration scenario, high speed and high load. Figure 3.11 shows histograms of the tri-axial accelerometer when the motor runs at 1600 RPM and with high compressor load. As can be seen, there is clipping in the signal in X- and Y-axis where the measured acceleration exceeds 6 g. There are some clipping of the signal in Z-axis as well, but not to the same extent as in the other two directions. Figure 3.12 is a similar test but with the compressor disconnected, in this case there is no no risk of clipping. This clipping effect ruins the signal and introduces high frequency disturbances in the signal, thus only the low frequencies should be regarded when analyzing the accelerometer data from X- and Y-axis with the compressor on.

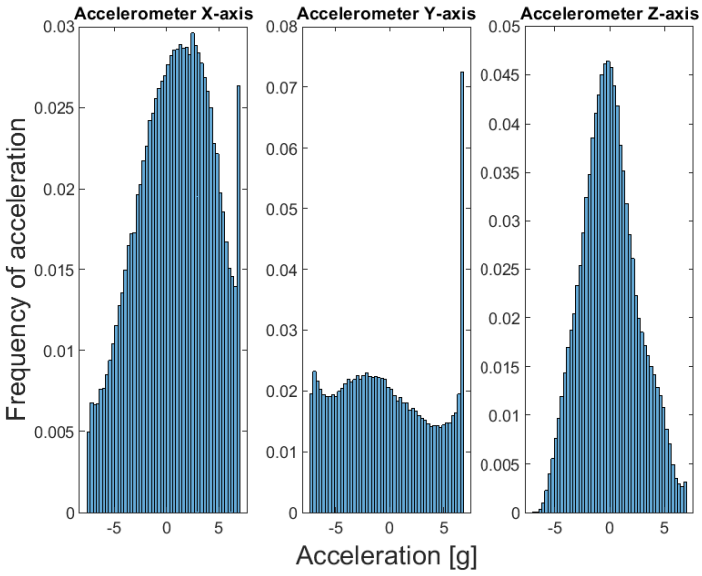

Figure 3.11: Histogram showing the effect of clipping. Done with $25 \cdot 10^5$ samples from the tri-axial accelerometer with the motor running at 1600 RPM and high compressor load.

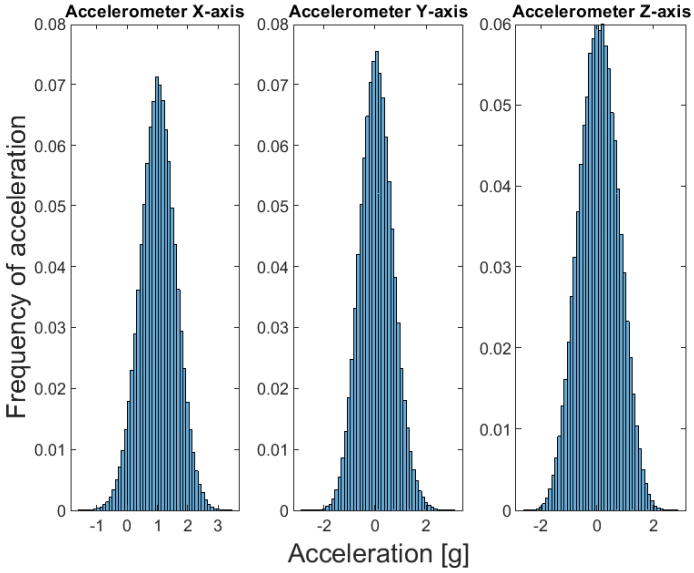

Figure 3.12: Histogram showing $25 \cdot 10^5$ samples from the tri-axial accelerometer with the motor running at 1600 RPM and no compressor load.

The vibrations from the compressor were measured on the compressor casing to characterize noise. The motor was set to run at 1590 RPM with high compressor load, settings that ought to be the most extreme in this context in terms of vibrations. The power spectral density plot is shown in Figure 3.13 and it seems like the vibrations in all three axes are periodical with the fundamental frequency 32.7 Hz, which corresponds to the compressor shaft's rotational frequency. Fundamental compressor shaft frequency $= \frac{1590 \cdot 1.24}{60} = 33$ Hz. Except the distinct periodic

components, the power increase around 600 Hz suggests that the compressor also produces a wide band noise. A 9th order Butterworth low-pass filter with cutoff frequency at 400 Hz was applied to allow for subsequent analysis of the low frequency accelerometer data.

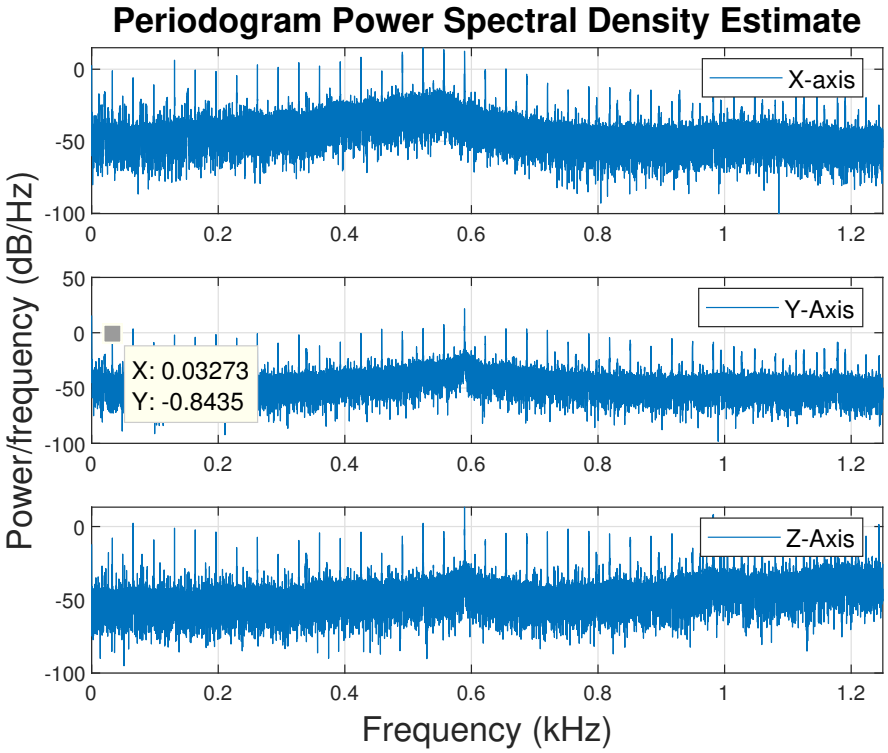

Figure 3.13: Power spectral density of the vibrations on the compressor. Clearly periodic with and increased power around 600 Hz.

3.6.5 Estimating clutch status from available sensors

The status the compressor clutch mentioned earlier was not measured but could be determined with an accuracy of a few seconds by combining the discharge pressure and drive current, using the fact that both are increasing when the clutch activates and both decrease when the clutch deactivates.

3.6.6 Data collection

The data was collected with a National Instruments DAQ-system using *LabView*. First the data was sampled with 10 kHz and 1 Hz for the fast and slow dynamics respectively. Due to the high amount of generated data, the 10kHz channel was reduced to 2.5 kHz. A test wast also done with the low frequency channel set to 10 Hz to see if it was possible to detect faster temperature and speed changes and differentiate them from outliers, the benefits were minimal though.

4

Results

This chapter presents all the results obtained based on the procedures and methods described in earlier chapters.

4.1 Slip in system and classification

With the photoelectric sensors it was possible to measure the speed of the compressor pulley and the motor pulley with an uncertainty of ± 20 RPM. By averaging over a longer period it was however possible to find a stable ratio between the motor and compressor speed.

By turning the compressor on and off multiple times it is possible to see that the tension of the belt affects the performance. By comparing high (300 lbf), normal (180 lbf) and low (50 lbf) tension in Figure 4.1, it is seen that when the compressor turns on the speed change differently. The clutch is initially activated for all the three cases, see subfigure 3 and then runs with a 30/10 cycle where it is on 30 seconds and then off 10 seconds. When tension is very high, around 300 lbf and the compressor turns on, the motor slows down and the current peaks, see the dips in $t = 45$ and $t = 75$ in the subfigures. With a tension that is very low, around 50 lbf it is possible to observe a speed loss on the compressor over the entire time it is on.

As seen in the Figure 4.1, the drive speed is similar for the tension levels, except of the dip when the clutch is activated with high tension. It is visible that the drive speed slightly increases with lower tension. The compressor speed is affected more and a $1 - 1.5\%$ drop is seen when the clutch is on. The hypothesis is that the slip occurs on the compressor side due to a smaller contact surface since the compressor pulley diameter is smaller than on the motor side. The decrease in RPM when the compressor clutch is activated when the tension is high might be because the added load is too high for the motor, causing it to slow down instead of slipping.

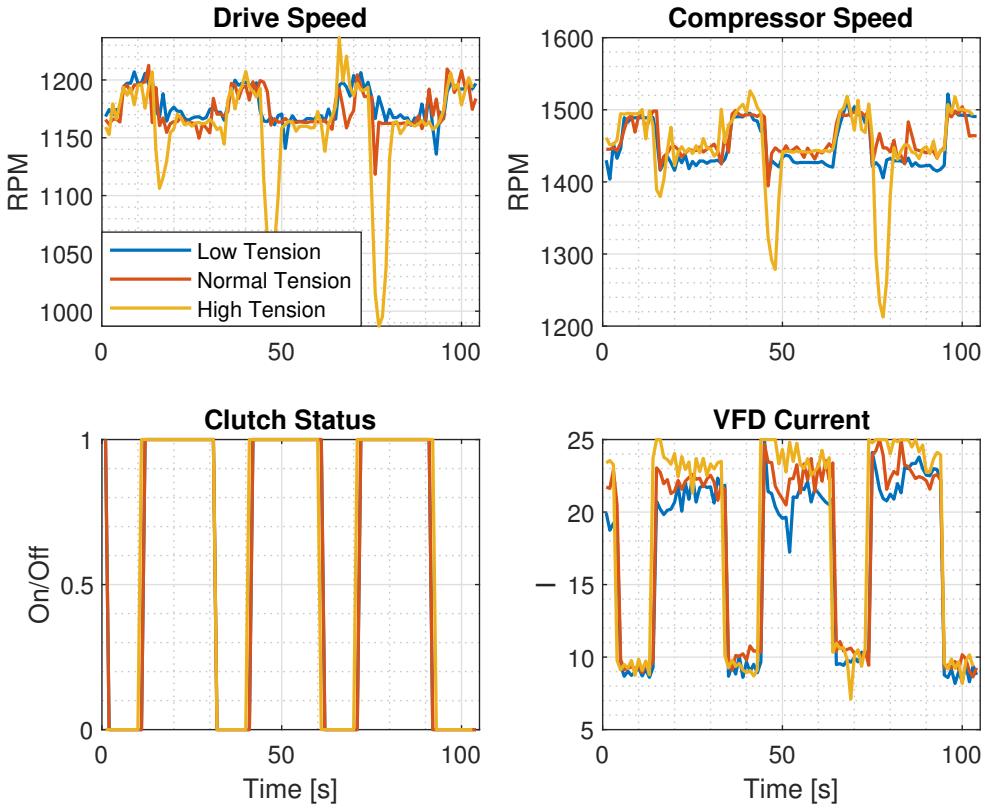

Figure 4.1: Raw data of compressor and motor speed when turning compressor clutch on and off for different tension with the motor set to 1200 RPM.

In Figure 4.2 the ratio

$$r = \frac{1}{L} \sum \frac{v_{comp}}{v_{drive}} \tag{4.1}$$

is displayed for 11 different tension levels and 3 different load levels.

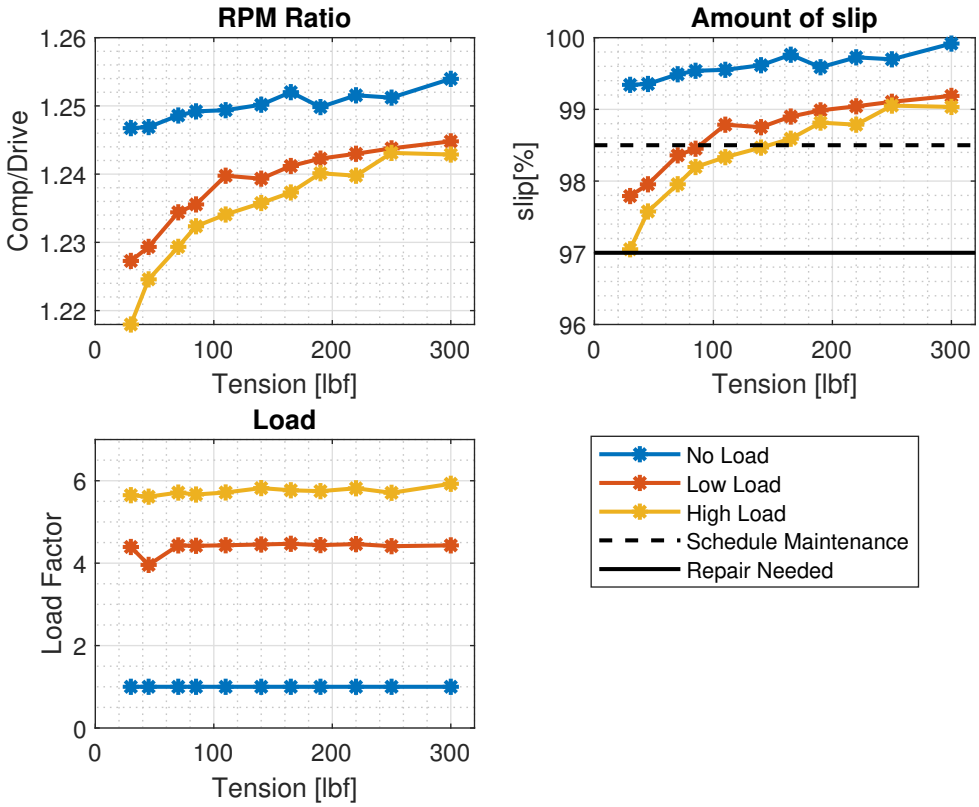

Figure 4.2: Slip occuring in the system when decreasing the tension from 300 lbf to 30 lbf for high load, low load and no load at 1200 RPM.

Figure 4.2 subfigure 1 shows that the speed ratio between the compressor pulley and the motor pulley decreases when the tension is lowered. That is, the compressor moves slower with respect to the motor which is a sign of increased slippage. The blue line shows a linear behavior for the different test but is likely to drop quickly when tension is decreased even more. By normalizing with the measured pulley ratio 1.255, a ratio is obtained which shows the amount of slip in the system, expressed as an efficiency loss where 1 corresponds to a perfect transmission with no slip, visible in subfigure 2. When the ratio is normalized, it is visible how slip occurs when a load is added, ranging from a loss between $1 - 3\%$. In the figure, the suggested lower level of slip is added as reference [11] where maintenance is suggested to be scheduled due to a slip level of 1.5% and where repair is urgent at 3%. If the ratio decreases much more, excessive heat may develop and the belt will wear out faster. Subfigure 3 shows the measured load factor for the three different load levels during the experiments.
Two functions are estimated, one for the case of no load, and one when load is added. By approximating the behavior using tension F_{belt} as input with

$$f(F_{belt}) = a + b \cdot log(F_{belt}) \tag{4.2}$$

where $a_1 = 0.9853$, $b_1 = 0.00224$ are parameters for no load and $a_2 = 0.9499$, $b_2 = 0.007351$ with load. To reduce the effect of different loads, visible in Figure

4.2, the ratio is slightly compensated with the load F_L as

$$r_{load} = r + (F_L - 5) \cdot 10^{-3} \tag{4.3}$$

The tension can then be estimated by solving the equation for tension, resulting in the equation

$$F_{belt} = e^{(\frac{r-a}{b})} \tag{4.4}$$

In Figure 4.3, the estimated tension from Equation 4.4 are shown where the ratio with load is compensated.

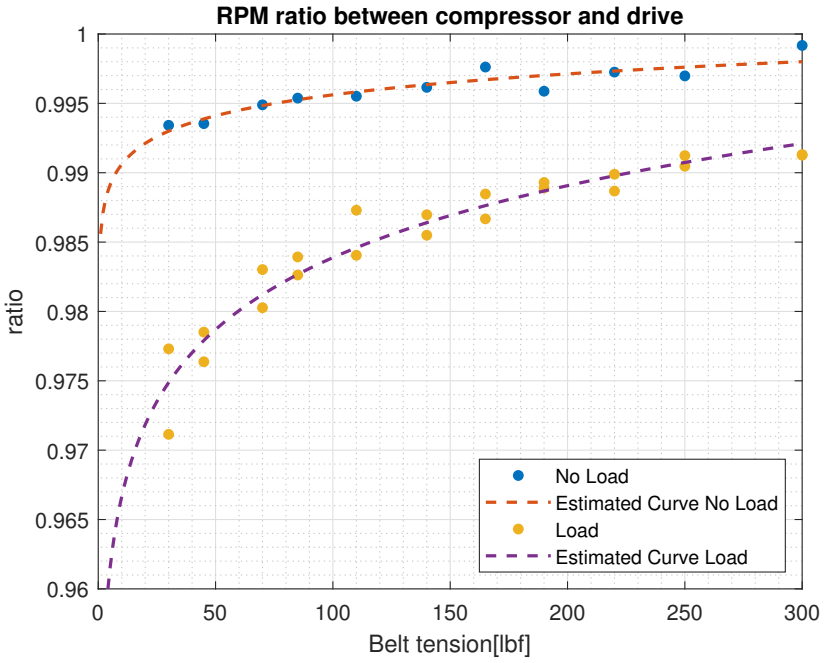

Figure 4.3: Slip occurring in the system while decreasing the tension from 300 lbf to 30 lbf for high load, low load and with the compressor disconnected at 1200 RPM.

The downside of this method is that it is dependent on a very accurate ratio measurement of the pulleys. By using the following method a metric that is less dependent on physical properties of the pulleys is obtained. As seen in Figure 4.1, the speed changes differently when the compressor is turned on dependent on the tension. By comparing the speed ratios

$$r = \frac{\frac{1}{N}\sum \frac{v_{comp,on}}{v_{drive,on}}}{\frac{1}{M}\sum \frac{v_{comp,off}}{v_{drive,off}}} \tag{4.5}$$

where M is the number of samples when the compressor is off and N is the number of samples with it is on, $v_{drive,on}$ and $v_{drive,off}$ is the speed on the motor side and $v_{comp,on}$ and $v_{comp,off}$ is on the compressor side in RPM, one gets a more general measurement that is independent on the pulley ratios, showing the loss when the compressor is turned on compared to when it is off. The relationship is shown in Figure 4.4.

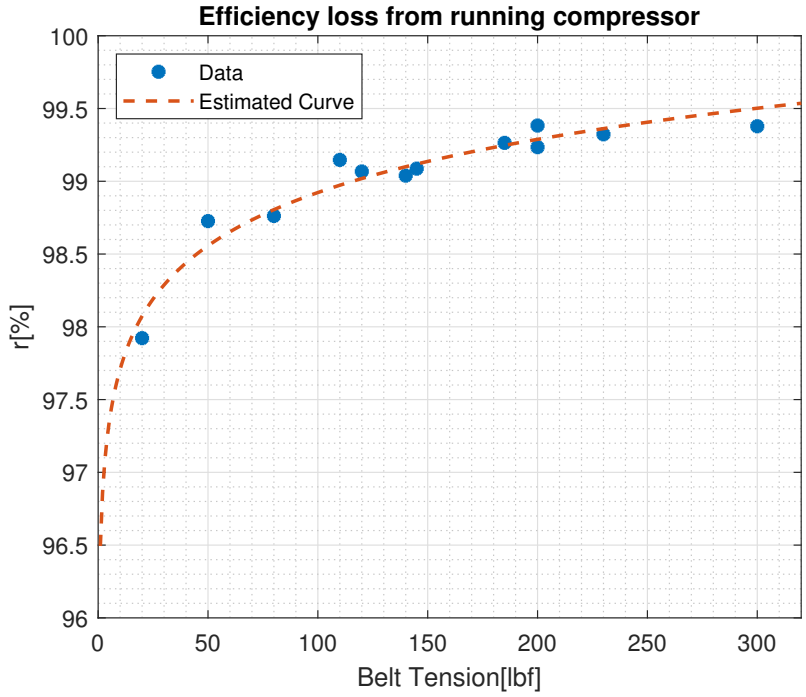

Figure 4.4: Tests comparing the speed ratio between the motor and the compressor pulley when the compressor clutch is activated and deactivated.

It indicates that the ratio is at most 99.4% with normal and high tension while it decreases faster under 100 lbf, down to 97.9% with the lowest tension of 30 lbf. With the recommended tension level of 180 lbf, it would be suggested to classify under 99% as low tension and under 98% as extremely low tension. Since the range of the classification only changes with 1.5% it is sensitive to disturbances and outliers in the signal, thus a longer period of time should be used. By minimizing the distance between the logarithmic function in Equation 4.2 and the data points, an estimated function valid for belt tension lower than 300 lbf is obtained where $a = 0.9649$ and $b = 0.005274$.

The results show that it is relatively easy to connect the speed ratio with the tension of the belts. What is remarkable is that the system performs well even with tension far lower than the suggested level of 180 lbf. This could be because the belt aging factor is not weighed in here, i.e just decreasing tension does not capture all conditions experienced by a belt in a real situation where it also suffers wear and tear, such as damaged and worn out teeth, cracks etc which might decrease the efficiency even more. In Figure 4.2, the case with no load seems to be linear which can of course not be the case when the tension is approaching 0. Since the used measurement tools couldn't measure under 30-50 lbf and due to the risk of damaging other components it was not possible to run tests with lower tension. It is however expected that the efficiency would have decreased rapidly for even lower levels.

The second method shows a result similar to the first one with the exception that it estimates the additional slip when adding a load and not total slip level. Dependent on the exact setup of the system, the initial slip might be higher and not detected by this method. The geometrical dimensions does not need to be known but the

downside is that the compressor clutch needs to be switched on and off at least one time to make an estimation.

4.2 Temperatures in pulleys and belts

From theory and observations, it was clear that the belt tension was directly influencing the developed heat in both the belts and the tensioner pulley where both low and high tension in theory should increase heat development.
With temperature measurements from the surface of the tensioner pulley, the compressor belt and the drive belt it was possible to compare how tension changed the steady state temperature of the components. Figure 4.5 shows the maximum temperature when running at 1600 RPM with the compressor disconnected

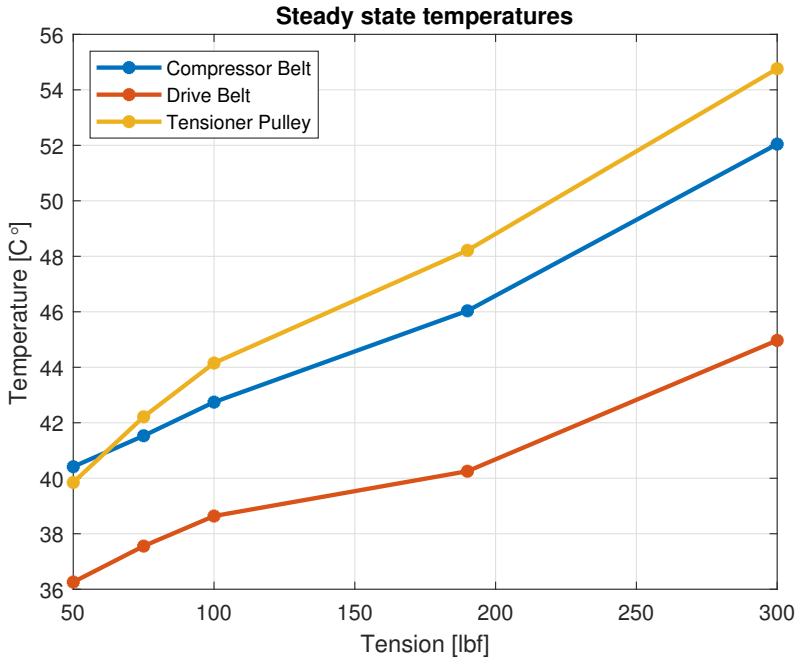

Figure 4.5: Steady state surface temperatures when running at 1600 RPM with compressor disconnected.

The figure shows that the temperature in the belts and the tensioner pulley monotonically increases with higher tension. The time duration to reach steady state temperatures was sometimes close to one hour, therefore limited tests of this kind was conducted.
By applying Equation 2.6 to estimate the temperature changes in the tensioner pulley, firstly by estimating the three material constants using a nonlinear least square solver(*lsqnonlin Matlab*) on the 9 tests defined for normal tension, the constants are estimated to $c_{tension} = 6.278 \cdot 10^{-5}$, $c_{air} = -3.508 \cdot 10^{-3}$, $c_v = 0.2956$. The estimated constants were then used in Equation 2.7, resulting in the tension predictions shown in Figure 4.6 when evaluating for the other 27 tests. With a correct prediction, the resulting tension estimate would lie on the dashed line in the figure.

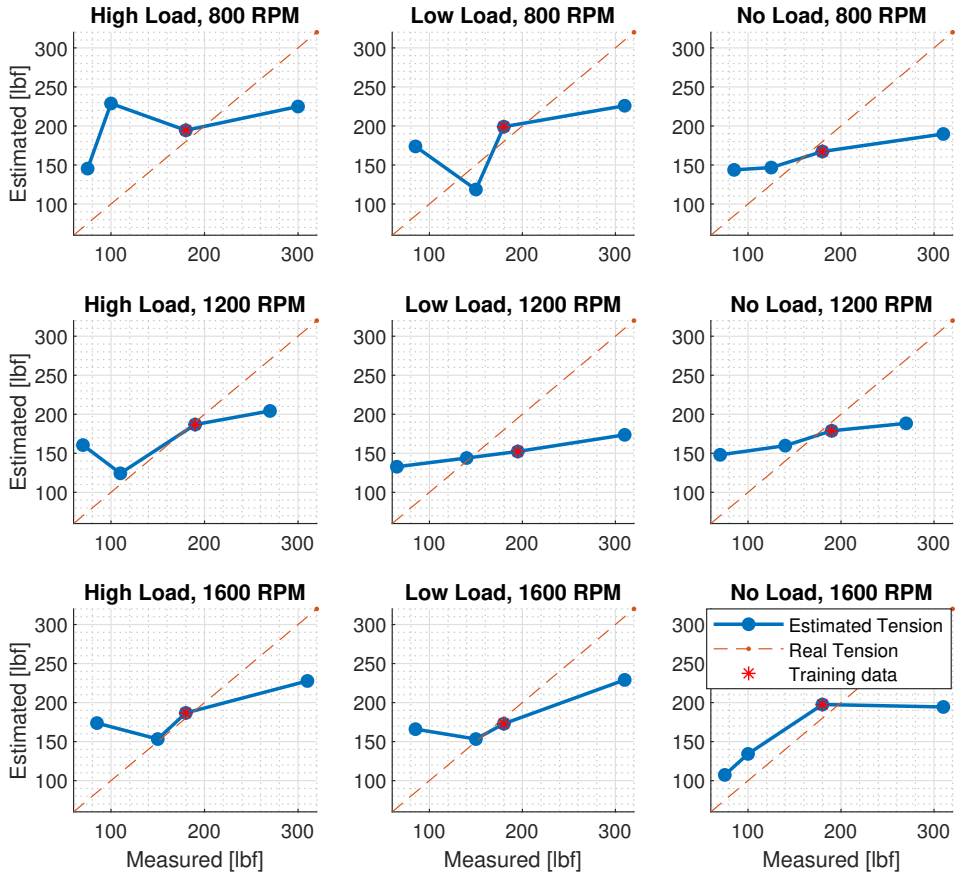

Figure 4.6: Estimated tension for the validation tests C1-C36 vs measured tension using the temperature model.

The results show that the tension estimates are slightly increasing with increasing true tension for most of the tests. However, the estimates are far from the true value especially for the highest and lowest tension.
It is possible that the results could have been improved with a more accurate model describing the system in more detail and utilizing other sensor measurements.
It is also possible that the tests used for the model are too short and contains information from old tests as stored heat in the materials. When the compressor has been used for a longer time, it gets hot and the temperature of surrounding air is heavily affected. Figure 4.5 shows the steady state temperatures which seems to increase quasi-linear over the measurement range. By conducting more tests during longer time, a better model could maybe have been derived.

4.3 Vibration analysis

This section presents the results focusing on the vibrations measured from an accelerometer. First the results from the method to detect waves in the belts are presented, followed by the results from kurtosis.

4.3.1 Transversal vibrations

To evaluate if the transversal wave, Equation 2.11, mentioned in section 2.4.3 can be found, the function is implemented and tested with the collected data. It could be possible to capture the wave with the laser interferometer, measuring the distance to the compressor belt but the idea is that it could also be detectable in the movement of the tensioner arm, measured by the accelerometer. If it is possible to find the frequency of the transverse wave, it would be possible to combine Equation 2.11 and Equation 2.10 in order to estimate the tension resulting in

$$F_{belt} = \frac{1}{2}(a^2 \pm \sqrt{a^4 + 4a^2 b} + 2b) \tag{4.6}$$

$$a = -2mLf\sqrt{\frac{\eta m V^2}{m}} \tag{4.7}$$

$$b = mV - \eta m V^2 \tag{4.8}$$

First a simple spectral analysis of a baseline test is done, in order to find candidate frequencies for the transversal wave. In Figure 4.7 the frequency spectrum from the laser interferometer and the accelerometer is shown while running at 1200 RPM, without the compressor and with tension 190 lbf. In the figure it can clearly be seen that the accelerometer shows content above 250 Hz while the laser interferometer does not. Since the interferometer primarily measures the compressor belt, it might be that content from the other components indeed lies in the higher range. By first studying the range 0-250 Hz, visible in the figure, one can see that there are many harmonics present, multiples of the natural frequencies.

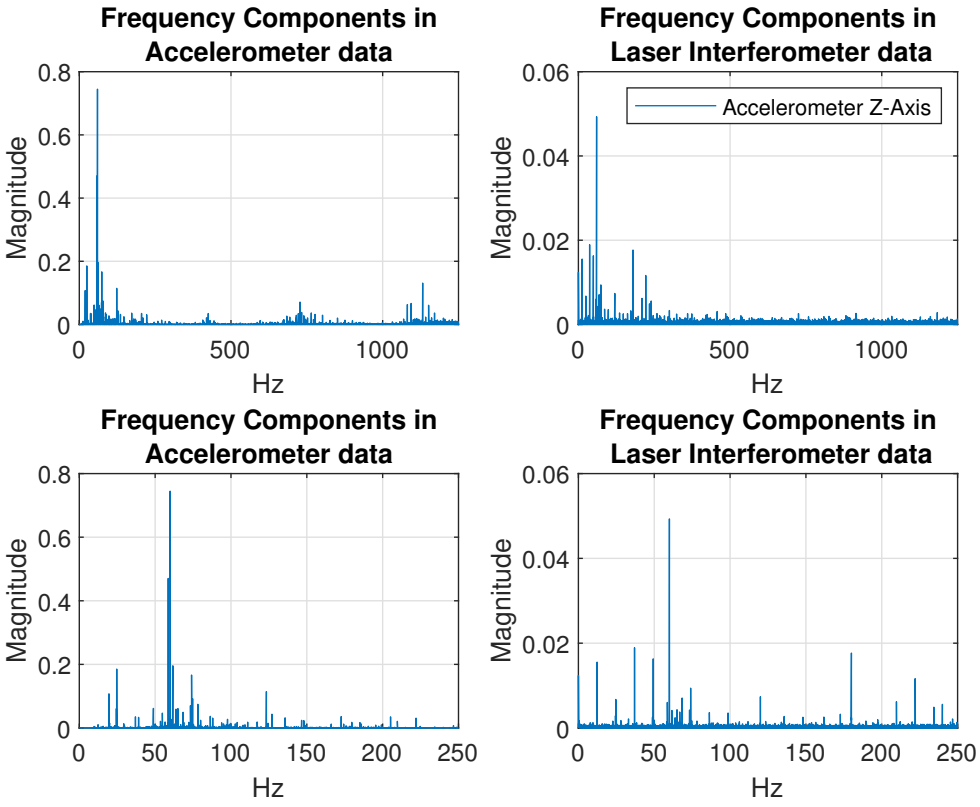

Figure 4.7: Frequency spectrum of test C6 at constant speed where the bottom subfigures are the top figures zoomed in on the range 0-250 Hz.

To be able to distinguish the transverse wave in the frequency spectrum, the natural frequencies of the data must be located and removed as potential candidates. Also noise related to the VFD(40 Hz) or power source(60 Hz) are removed. Since the accelerometer is the sensor that is under investigation, the laser is primarily used as reference data.

As expected, some of the dynamics of the system is seen in the frequency analysis of the measurements. In Figure 4.8, the fundamental frequencies related to the moving parts are highlighted. The test was done at 1194 RPM drive speed and 1495 RPM compressor speed according to the RPM sensors. The peaks $A = 9.78$ Hz and $B = 12.35$ Hz corresponds to the frequency of the drive belt and compressor belt respectively. $C = 2A$ is the first harmonic of the drive belt, $D = 19.96$ Hz corresponds to the frequency of the drive pulley $19.96 \cdot 60 = 1198RPM$, $E = 24.43$ Hz corresponds to the frequency of the tensioner pulley $24.43 \cdot 60 = 1465$ RPM, compressor harmonic $F = 2B$, lastly, $G = 24.89$ Hz is the speed of the compressor pulley $24.89 \cdot 60 = 1493$ RPM.

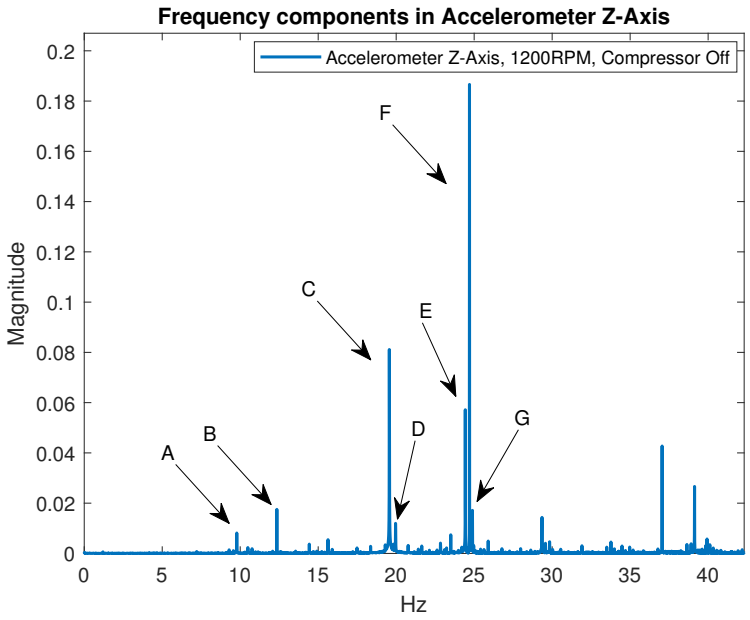

Figure 4.8: Frequency components in the tensioner arm measured by the accelerometer up to 40 Hz with the compressor clutch disconnected, running the motor constant around 1194 RPM. Fundamental frequencies are found in $A = 9.78$ Hz, $B = 12.35$ Hz, $D = 19.96$ Hz and $E = 24.43$ Hz and $G = 24.89$ Hz.

Table 4.1 shows the estimated frequency derived from (2.11) of the transverse wave for all tests defined in Table 3.7, calculated for the drive belt and compressor belt using $\eta = 0.7$. The frequency of the compressor belt is calculated with a 30 lbf higher tension than the drive belt, according to experiments. From the results it is suggested that the frequency is between 23.24-61.54 Hz for the drive belt and 41.64-89.56 Hz for the compressor belt, which results in a wide range to investigate.

Test	Drive[Hz]	Comp[Hz]	Test	Drive[Hz]	Comp[Hz]
A1	28.27	47.60	C1	46.36	69.79
A2	30.59	50.31	C2	46.31	69.72
A3	30.43	50.11	C3	46.16	69.52
A4	24.54	43.12	C4	45.75	68.96
A5	23.24	41.65	C5	46.39	69.78
A6	24.26	42.78	C6	45.55	68.70
A7	24.69	42.88	C7	41.75	63.78
A8	24.63	42.80	C8	41.70	63.70
A9	30.94	50.78	C9	41.53	63.48
B1	33.62	53.92	D1	60.51	88.21
B2	41.92	64.15	D2	61.65	89.71
B3	37.84	59.06	D3	61.54	89.57
B4	33.01	53.05	D4	55.72	81.90
B5	38.20	59.43	D5	60.07	87.61
B6	38.03	59.21	D6	55.56	81.68
B7	37.00	57.79	D7	58.03	84.89
B8	37.06	57.86	D8	57.99	84.83
B9	35.73	56.50	D9	57.84	84.63

Table 4.1: Estimated frequency of transverse wave using Equation 2.11 with η=0.7.

From the results in Table 4.1, test C6 shows that a wave should be present at 45.55 Hz and 68.70 Hz for the drive belt and compressor belt respectively. In Figure 4.9 the estimated frequency for a given tension in test C6 is shown.

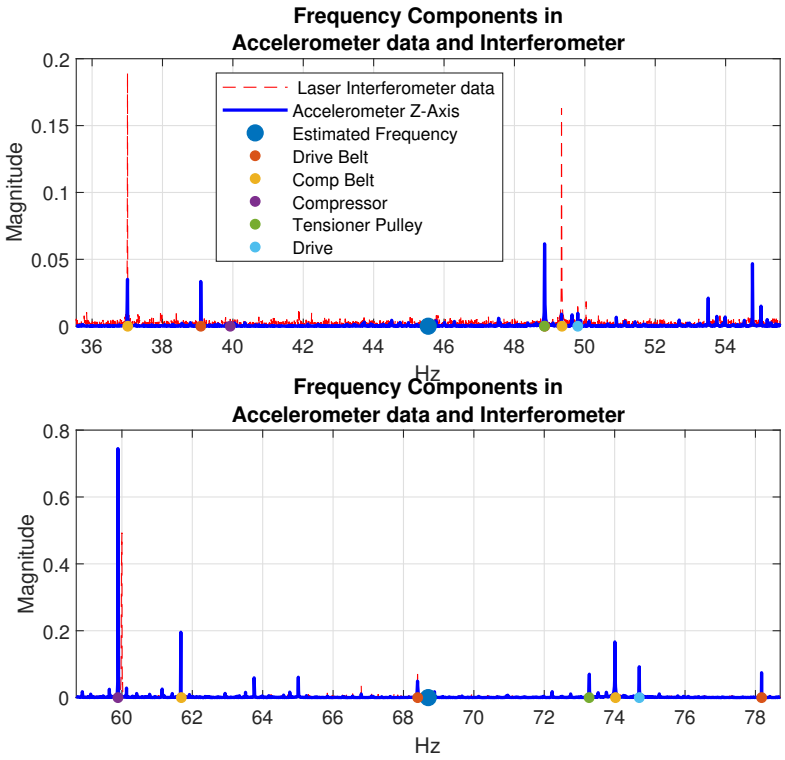

Figure 4.9: Data from test C6, estimated frequency range for the transverse wave in the belts. Upper figure shows the drive belt and bottom figure the compressor belt. The harmonics of the known components are added in the figure.

Since a lot of content is shown in the frequency plots, often harmonics of the five components mentioned before, an algorithm to rule out harmonics is used. For each test the five fundamental frequencies are estimated using the RPM measurements as reference. The fundamental frequencies of the belts are found from $f_{belt} = \frac{1}{2}\frac{v_{belt}}{60} \pm 1$ Hz, $f_{comp} = \frac{1}{2}\frac{v_{comp}}{60} \pm 1$ Hz since the belt lengths are roughly 2x the pulley radii. The drive frequency from $f_{drive} = \frac{v_{drive}}{60} \pm 1$ Hz, compressor frequency and tensioner pulley frequency as the two largest peaks in $f_{comp} = \frac{v_{comp}}{60} \pm 1$ Hz not equal to the second harmonic of the belt. By finding all peaks in the range 30-100 Hz larger then magnitude M and then calculating the rest when dividing with the five fundamental frequencies, peaks that are not related to the physical components are found. In Figure 4.10 the results for the two largest peaks for the 36 tests are shown using Equation 4.8.

The results does not clearly show the frequency peaks that were estimated and presented in Table 4.1. In order to use the method these predictions would have been needed to be more accurate. In the figure it is visible that some of the estimates are close to the prediction, however most are far away which would have resulted in bad tension estimates. It is therefor no idea to further continue develop the proposed method.

The results might be limited due to the fact that the belts are too short for a distinguishable wave to appear. Since the accelerometer and laser interferometer captures vibrations from every possible source, the sought wave may be lost due to

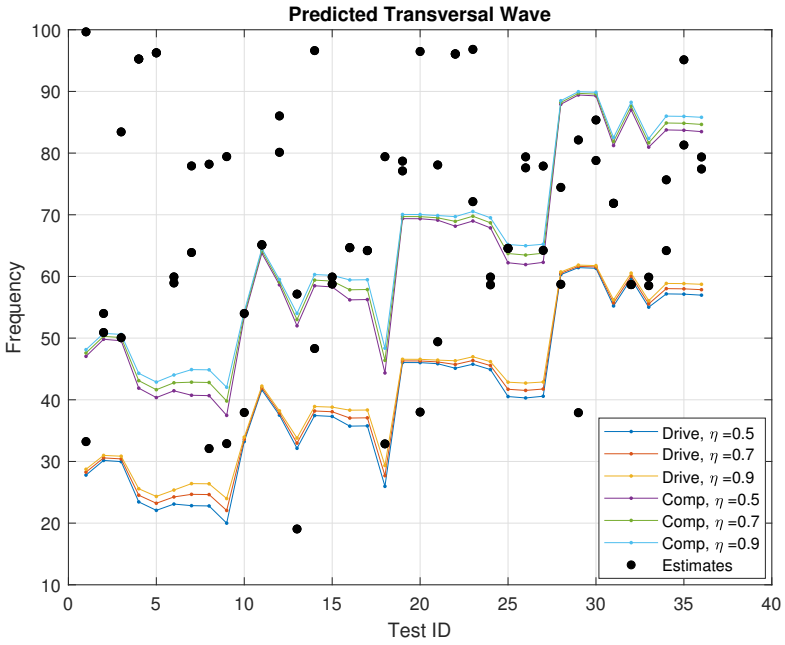

Figure 4.10: Results of the two largest peaks for each test found in the accelerometer data using Equation 2.11 with η=0.5-0.9.

interference with other vibrations, making it undetectable during certain conditions. One other weakness of the method is that it is highly dependent on dimensions of the radii and belts in the system. Furthermore it also relies on piece-wise constant speed.

4.3.2 Kurtosis

The kurtosis was calculated in different ways in every operating point to see how well it can be used to determine belt tension. The data used in these evaluations were only from the accelerometer's Z-axis, since the data from the other two axes were severely altered due to clipping, which immediately affects the kurtosis. To get enough samples, the kurtosis was evaluated every four seconds (10000 samples) in each of the operating points A1 through D9. The kurtosis was also calculated for the complete data set to see how much the sample size affects the result. Figure 4.11a shows the kurtosis of all samples and Figure 4.11b shows the median kurtosis from each operating point split into four seconds intervals. Each bar corresponds to a tension and each of the nine groups of bars corresponds to a speed and a load, where number 1 is high load and low speed, for example (compare with Table 3.7). The first thing to note is that there is practically no difference between the two cases, which can lead to the conclusion that the kurtosis is stable in steady state operations, it does not change over time and 10000 samples seems to be sufficient. The second thing to note is that there is no clear trend in the data.
As indicated in the theory, it could be interesting to look at the kurtosis in specific frequency bands. Instead of looking at an arbitrary band (or the octave bands as recommended by B. Fazedna et.all [3]), the band is here defined as the fundamental

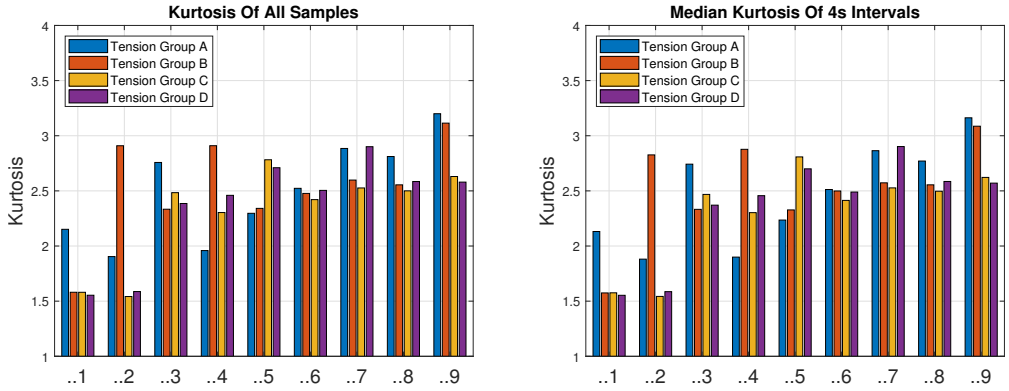

(a) Kurtosis of the complete time series.

(b) Median of intervals of 4 seconds (10000 samples).

Figure 4.11: Comparison of kurtosis for entire test and median of time intervals.

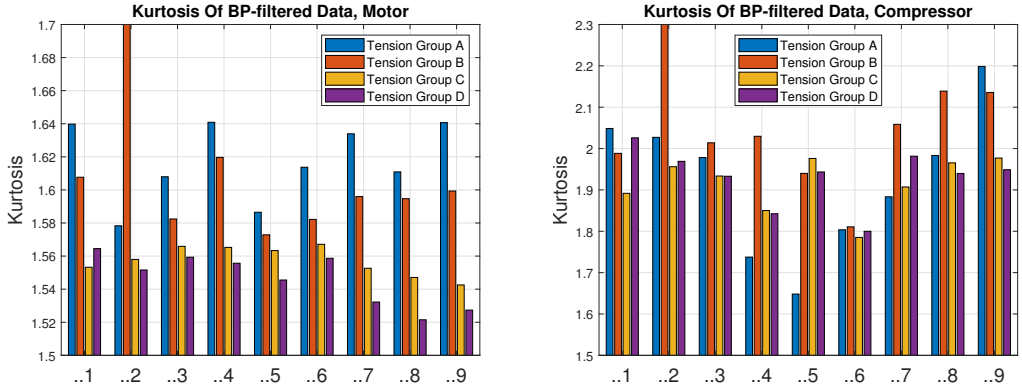

(a) Kurtosis of bandpass filtered accelerometer data with motor rotation as center frequency.

(b) Kurtosis of bandpass filtered accelerometer data with compressor rotation as center frequency.

Figure 4.12: Comparison of kurtosis filter with different BP-filters.

rotational frequency ± 3 Hz. This ought to capture variations in the vibrations related to machine rotation. Here the evaluation was done on the whole time series in each operating point and after being bandpass filtered with a 3rd order Butterworth filter. Both the motor's and the compressor's speed were tested as center frequencies when designing the bandpass filters. The plots in Figure 4.12a and 4.12b shows the kurtosis of the bandpass filtered data in each operating point.

Here are some truly interesting results, there is a clear trend showing decreasing kurtosis for increased tension, when looking at the case with motor speed centered BP filtering. There are only two instances that does not follow the trend; B2 and D1. By reviewing experiment notes, it was discovered that the accelerometer was not properly mounted when collecting the data for B2, making it useless in this context. No reason could be found to why D1 does not conform to the trend. Why the motor speed suits as a better foundation for the BP filtering with this application is not easy to say, but a guess is that there are more frequency components close to the compressor's fundamental rotational frequency, thus the BP filter is unable

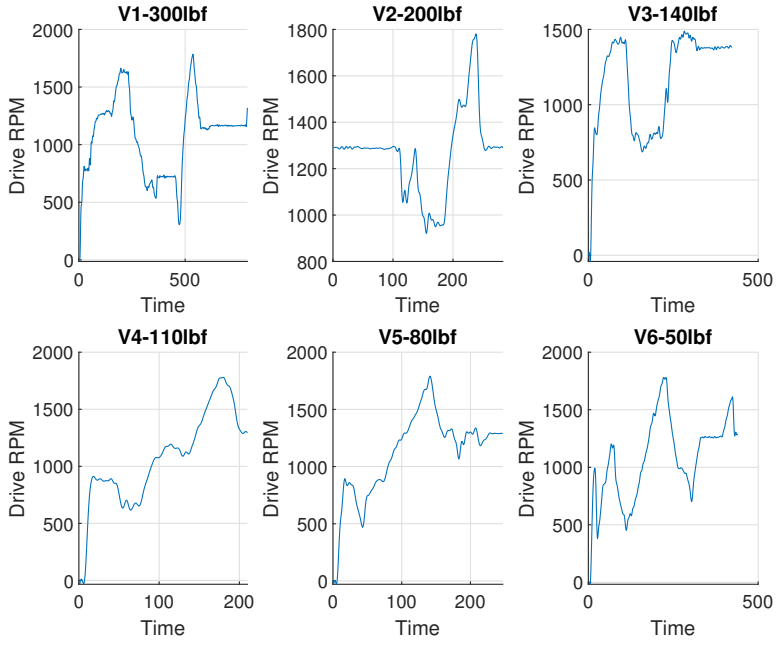

Figure 4.13: RPM over time for verification tests V1-V6.

to single out just the component related to its rotations. Given the first results, that the kurtosis of the vibrations in steady state can be considered constant, the kurtosis values produced here could potentially be used as a baseline calibration when determining tension. Although the trend is clear, the difference from one operating point to the next is very small and will probably be a cause for error when trying to classify tension.

4.4 Verification

In order to verify the correctness of the methods, tests that were not used when deriving the methods are used as verification. The verification tests ranges from tension 50-300 lbf with varying drive RPM and load, an attempt to mimic realistic behaviour of a climate system in a bus. The details of the tests are visible in Figure 4.13 and Figure 4.14 showing the RPM and load respectively. The tension of the belt is divided into four different levels(A,B,C,D) defined in Table 3.3 with C as the normal level where each method is validated for all test cases. The results of the methods are shown in Table 4.3.

4.4.1 Slip

The first slip function was evaluated on the verification tests by calculating the median of the speed ratio. The case with load(a_1, b_1) and no load(a_2, b_2) was calculated separately and then Equation 4.4 was used to get a weighted tension estimate with respect to the number of data points in the two different cases. The results in Table 4.3 shows that the method can cope with both varying speed and

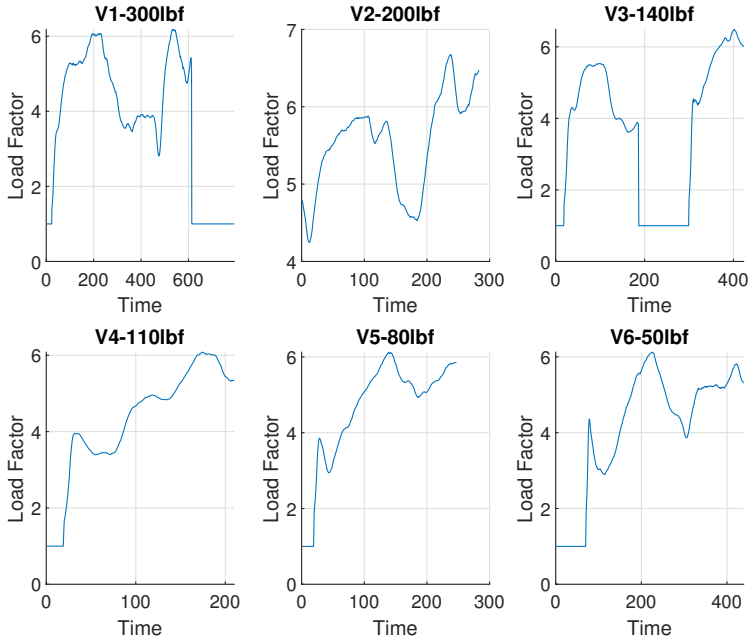

Figure 4.14: Load over time for verification tests V1-V6.

load and still achieve good estimates. Test V2 is the only case where the results are closer to another classification.
The second slip function was evaluated by taking the mean of the speed ratios in Equation 4.2. In V2 the compressor was always on, resulting in lack of information for the method. In test V3 and V4 the method resulted in unrealistic estimates, showing the lack of robustness for this method.

4.4.2 Temperatures

The temperature model was evaluated by estimating tension every second according to Equation 2.7 and then using the mean of the results to classify tension. In Figure 4.6 it is shown that the estimations are only accurate close to 180 lbf but in the verification results the tension is estimated between 244-271 lbf for all tests.

4.4.3 Kurtosis

The verification was done by splitting the verification tests into 4-seconds intervals and then finding the speed and load combination that lies closest to any of the nine predefined combinations. Then the calculated kurtosis value was compared to the corresponding kurtosis value for that speed and load combination with the baseline and thus could be connected to a tension class. Table 4.2 shows the resulting classification based on the described method. It is clear that the resulting classification is non-informative, with most of the calculations giving a kurtosis value higher than in the baseline(resulting in group A) and the rest are below the baseline (resulting in group D). None of the verification tests end up with a kurtosis value

Verification number	Correct tension class	Classification results
V1	D	144xA 4xD
V2	C	60xA 9xD
V3	B	85xA 9xD
V4	B	32xA 7xD
V5	A	45xA 6xD
V6	A	73xA 11xD

Table 4.2: The resulting classifications made by comparing the kurtosis of vibration measurements in to a baseline. The classification results indicates the number of times a tension class is found through out the entire length of the verification tests.

within the relatively small gap in the baseline that would have resulted in a C or B classification.

		Methods				
Test	Tension	RPM slip	RPM comp on/off	Kurtosis	Vibrations	Temperature
V1	300/D	293/D	279/D	A	-	262/D
V2	200/C	266/D	$*^1$	A	-	259/D
V3	140/B	132/B	>300	A	-	244/D
V4	110/B	127/B	>300	A	-	271/D
V5	80/A	87/B	89/B	A	-	265/D
V6	50/A	56/A	33/A	A	-	249/D

Table 4.3: Classification results for the developed methods, test with $*^1$ does not contain enough information for the algorithm.

5
Conclusion

The results showed that one of the simpler methods, i.e slip estimation by comparing the speed ratio of the drive and the compressor also gave the most accurate results. It has a direct connection to the performance of the system and there are guidelines where maintenance should be scheduled for a certain percentage of slip. The method also only uses two speed sensors, with optional use of a clutch sensor and pressure sensors, making it simple to implement.
The developed temperature model proved to be very inaccurate and the model assumptions are probably not valid based on the results. In hindsight, the data on which the model parameters were estimated, could probably have been produced in a more clinical way, by being more cautions about ambient temperature, lingering heat from previous experiments and better ability to reach temperature steady state. When the model was applied on steady state operation points in Figure 4.6, a small tendency of higher tension estimate for higher measured tension was observed. When evaluating on the six verification tests with varying load and speed, the method predicts very high tension for all cases and does not seem to show any trend.
The idea to identify a transverse wave in the belt, directly connected to the tension of the belt according to theory was not possibly to finalize. The method was dependent on that frequency peaks of relatively high magnitude could be found by the accelerometer or laser interferometer data and distinguished from other content, which wasn't the case. There are several likely reasons to why these vibrations were not found. First of all, the model used to localize the frequency components might be to simple or even invalid in this case. Another possibility is that he model is valid but vibrations from other parts are of such high magnitude that it is impossible to find the sought frequency components.
Kurtosis of bandpass filtered vibrations did indeed show some very interesting results, there was a clear difference between different tensions just as indicated by earlier research. Also similar to previous studies, no good reason could be found to explain why this trend is present in some frequency bands. Even though the differences are visible when comparing tension cases side-by-side, it was not possible use these small differences as a base for calibration to tell what is good and what is bad. Kurtosis could on the other hand be a good candidate as potential parameter to observe over a long period of time, to monitor slow degradation.
The quality of the results might have been limited by the design and construction of the test rig. In order to obtain general results which can be applicable to a similar system in it's natural environment, i.e inside a vehicle, one must be very cautions about what differs the mock-up from a realistic implementation. There are several things in the test rig built for this work that differs from what one would expect

from a system implemented in a vehicle. First thing is the electric motor, in a real system of this kind a diesel engine would be used, adding a lot of other vibrations and heat dynamics. The installation and alignment of pulleys was here done by hand while professional technicians uses sophisticated laser tools. This possibly improper alignment of rotating biddies might have given rise to powerful vibrations. The compressor and motor was mounted on the same rigid steel base, which means that vibrations from all parts of the rig are well merged, compared to a real system where some parts might be isolated but other vibration disturbances are introduced. The way the air is flowing around the rig might also have caused loss of generality. The warm and cold air produced by the rig were not channeled away, thus creating a great deal of trouble when trying to reach steady temperatures. Experiments showed that even after one hour with the compressor operating in steady state, it was not enough to reach steady temperatures on the belts or the pulley bearings. Since the rig itself changes the ambient temperature arbitrarily without any control or reference, it's natural that temperatures settles very slowly.
Another source of disturbance that was very hard to precisely define and even more so to eliminate was the resonance experienced at certain motor speeds. At these speeds the belt started to oscillate violently and the lower the tension the higher the belts oscillating amplitude. Since these oscillations appeared at different speeds and with different magnitude for any given tension, it is impossible to tell where it impacted any other measurements and where it didn't.
Future work within the area of predicting the conditions of belts in a power transmission should be done in a system more similar to that in which it is intended to be implemented. The future focus should also be on collecting data over a longer period of time, from installation to replacement of the worn out belt, to capture the gradual degradation. In this work, the belt's tension is completely decoupled from its degradation and wear, which in reality are two dependant factors. The combination of more data and a more realistic system could then be a good foundation for using other approaches, either go more in depth into one or several of the methods shown here or use an even more data driven approach with a machine learning solution. If the former is pursued, a recommendation is to do belt tension diagnostics by finding operating points and metrics that in combination gives a reliable tension indication. From there it is all about calibration to find the boundaries of these metrics, within which the tension is acceptable.
All in all, this work have utilized simple methods in an attempt to classify belt tension based on properties that are related to the tension of a power transmission belt. As mentioned in the introduction, there is currently no known way of determining belt tension of a running belt, and this work has just emphasized the difficulties of performing that task. Perhaps one of the biggest drawbacks of the approach taken in this work is the lack of an in depth development of one specific method and analysis of the corresponding belt properties. One could for example easily focus an entire thesis on just looking at what is causing the belt to vibrate and how to capture the behaviour in the best way. On the other hand, this way of confronting the problem from several directions can still provide insight into the matter, knowledge that hopefully can be used when deciding where future effort should be put.

Bibliography

[1] "Analyze your way to longer lasting better performing v-belt drives power transmission division." Gates Corporation, 2010.

[2] Y. Hu, Y. Yan, L. Wang, X. Qian, and X. Wang, "Simultaneous measurement of belt speed and vibration through electrostatic sensing and data fusion," *IEEE Transactions on Instrumentation and Measurement*, vol. 65, pp. 1130–1138, May 2016.

[3] B. Fazenda, F. Gu, M. Avis, and A. Ball, "Measurement and diagnostic of engine belt physical condition from acoustic signals," in *2009 ICCAS-SICE*, pp. 2062–2067, Aug 2009.

[4] T. J. Kang, C. Yang, Y. Park, S. B. Lee, and M. Teska, "Electrical monitoring of mechanical defects in induction motor driven v-belt-pulley speed reduction couplings," in *2017 IEEE Energy Conversion Congress and Exposition (ECCE)*, pp. 293–300, Oct 2017.

[5] A. Picot, E. Fournier, J. Régnier, M. TientcheuYamdeu, J. M. Andréjak, and P. Maussion, "Statistic-based method to monitor belt transmission looseness through motor phase currents," *IEEE Transactions on Industrial Informatics*, vol. 13, pp. 1332–1340, June 2017.

[6] J. Shepherd, "Hot and cold running belts." Power Transmission Design Magazine, October 1992.

[7] S. E. Bechtel, S. Vohra, K. Jacob, and C. Carlson, "The stretching and slipping of belts and fibers on pulleys," *Journal of Applied Mechanics*, vol. 67, pp. 197–206, September 1999.

[8] SKF, "The SKF model for calculating the frictional moment."

[9] Z. Liang, J. Wei, J. Zhao, H. L. anf B. Li, J. Shen, and C. Zheng, "The statistical meaning of kurtosis and its new application to identification of persons based on seismic signals," *Sensors*, vol. 8, p. 5106–5119, August 2008.

[10] K. D. Rao and M. N. S. Swamy, *Digital Signal Processing Theory and Practice*, ch. 5. Singapore: Springer Nature, 2018.

[11] R. E. Brown, "The development of an electronic system to continually monitor, indicate and control, 'belt slippage' in industrial friction 'v' belt drive transmission systems," *Journal of Physics: Conference Series*, vol. 364, no. 1, p. 012055, 2012.